SAND REPORT
SAND 2002-2801
Unlimited Release
Printed August 2002

The Formation and Evolution of Plasmas from Single Exploding Wires

Final Report for Sandia Project 22995 "Single Wire Explosion Experiments"

David Hammer, P. U. Duselis, Min Hu, and Bruce Kusse

Prepared by
Sandia National Laboratories
Albuquerque, New Mexico 87185 and Livermore, California 94550

Sandia is a multiprogram laboratory operated by Sandia Corporation, a Lockheed Martin Company, for the United States Department of Energy under Contract DE-AC04-94AL85000.

Sandia National Laboratories

Issued by Sandia National Laboratories, operated for the United States Department of Energy by Sandia Corporation.

Available to DOE and DOE contractors from
U.S. Department of Energy
Office of Scientific and Technical Information
P.O. Box 62
Oak Ridge, TN 37831

Telephone: (865)576-8401
Facsimile: (865)576-5728
E-Mail: reports@adonis.osti.gov
Online ordering: http://www.doe.gov/bridge

Available to the public from
U.S. Department of Commerce
National Technical Information Service
5285 Port Royal Rd
Springfield, VA 22161

Telephone: (800)553-6847
Facsimile: (703)605-6900
E-Mail: orders@ntis.fedworld.gov
Online order: http://www.ntis.gov/help/ordermethods.asp?loc=7-4-0#online

SAND2002-2801
Unlimited Release
Printed August 2002

Distribution
Category UC–706

The Formation and Evolution of Plasmas from Single Exploding Wires

Final Report for Sandia Project 22995 "Single Wire Explosion Experiments"

David Hammer, P. U. Duselis, Min Hu, and Bruce Kusse
Cornell University Laboratory of Plasma Science
Ithaca, NY

Abstract

In this report we describe a series of single wire explosion experiments that have been performed at Cornell's Laboratory of Plasma Studies. Wires of Ag, Cu, Au, Al and W, 1 to 3 cm in length and 10 to 25 microns in diameter, were driven by a ~100ns current pulse with a current rise time of approximately 30 A/ns. Previously, it has been found that the wires, in general, experienced a 50-85 ns resistive heating phase that was terminated by a rapid collapse of voltage [[1]]. We attribute this voltage collapse to the formation of a coronal plasma around the wire core. In order to understand this plasma formation and its effect on the voltage collapse, experimental observations of plasma radiation from single wire explosions have been made with an optical framing camera as well as UV and optically sensitive diodes. The temporal and spatial dynamics of the plasma expansion were observed. The relative timing of the voltage collapse and the radiation was examined.

[1] D. B. Sinars, Min Hu, K. M. Chandler, T. A. Shelkovenko, S. A. Pikuz, J. B. Greenly, D. A. Hammer, and B. R. Kusse, "Experiments measuring the initial energy deposition, expansion rates and morphology of exploding wires with about 1 kA/wire", Physics of Plasmas 8, pp216-230.

Contents

Figures

INTRODUCTION

Single wires of Ag, Cu, Au, Al and W, 1 to 3 cm in length and 10 to 25 μm in diameter, were driven by a 100 ns current pulse with a rate of rise of the current of 20 A/ns. Earlier experiments found that the wires generally experienced a 50-85 ns resistive heating phase that was terminated by a rapid collapse of voltage [1]. This voltage collapse was attributed to the formation of a coronal plasma around the dense wire core that was observed with x-ray backlighting [1].

For this project, observations of the plasma formation around the time of voltage collapse were made using two new diagnostics: 1) A vacuum diode sensitive to UV radiation with 1-5 nsec response time, and 2) A visible light framing camera with a 1-50 ns shutter. The vacuum diode gave time-resolved measurements and the framing camera gave spatially resolved measurements with a time resolution limited by the shutter speed.

The vacuum diode showed no UV radiation until the moment of voltage collapse, at which time a 5-10 ns burst of radiation was observed. After this collapse low level UV radiation was detected as the current continued to rise. These observations are consistent with the picture that the voltage collapse is caused by the formation of plasma around a core of neutral wire material causing a transfer of the current from the wire material in the core to the surrounding plasma.

The framing camera was used to obtain spatial resolution of the emitted UV radiation. By changing the timing of the frame relative to the start of the current pulse, the plasma radius as a function of time was obtained. Radial expansion rates from the framing camera were similar to those obtained by interferometry in previous experiments: 3 μm/ns from the framing camera and 2.5 μm/ns from interferometry. However, the framing camera appeared to be more sensitive to the lower plasma densities than was the interferometer. Just after voltage collapse the framing camera results showed the existence of plasma at a larger radius than did the interferometer. Using the framing camera results, it was possible to calculate a plasma column resistance based upon Spitzer resistivity that was comparable to the resistance value obtained from the experimental current-voltage data. This further confirms the idea that the voltage collapse in exploding wire experiments is caused by the formation of a coronal plasma around the dense, neutral wire core material that we observe with x-ray backlighting.

CAMERA LIMITS

A. Spatial Resolution

The entrance of the framing camera has a resolution of 3 lines / mm at 50% contrast. The loss of resolution occurs at the interface between phosphor screen and the fiber optic bundle (Figure 1). The glass screen between the two blurs a point of light on the phosphor screen to a width equal to the thickness of the glass. The experiment uses a simple lens to magnify the image of the wire by a factor of 5.1 to give a resolution of 15 lines / mm. To test the resolution of the system, a Ronchi grating with 50 μm lines was imaged. The framing camera with the lens was able to image the Ronchi grating at slightly better than 50% modulation. The walls of the vacuum system that contain the exploding wire limit the magnification that one can conveniently use. A

lens with a reasonable f# was mounted as close as possible to the wire but still remained outside the vacuum system.

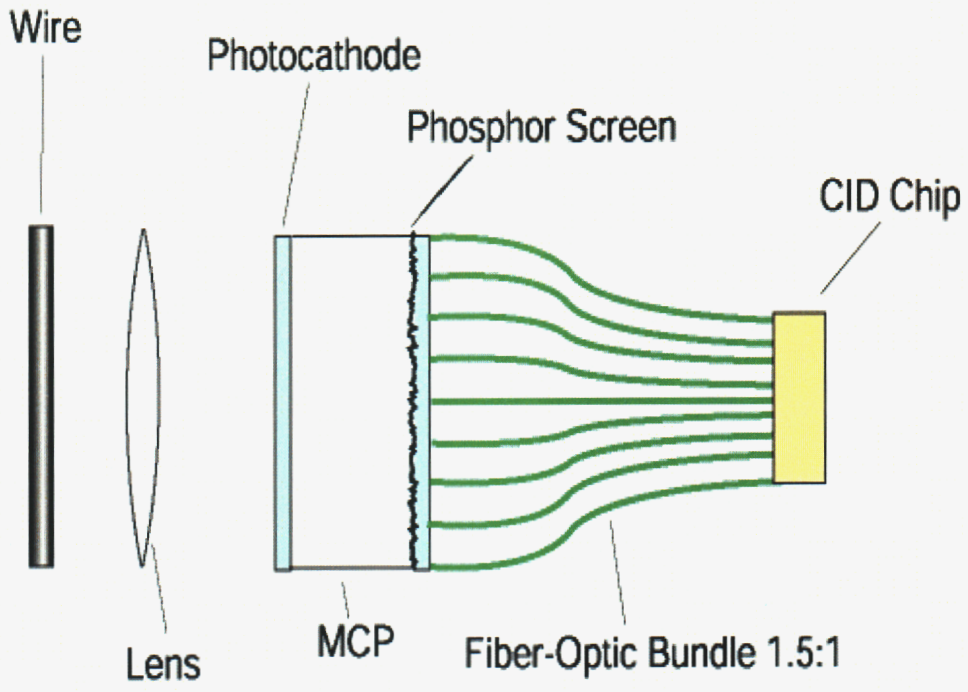

Figure 1. Framing camera geometry.

B. Time Resolution

The framing camera itself generates a signal that is supposed represent the camera trigger monitor. By using a 4 ns long laser pulse, the trigger monitor signal was calibrated. The fastest shutter speed of this camera was determined to be 8.4 ns ± 0.4 ns. The shutter speed is easily lengthened to any time with simple modifications. For almost all the data that appears on this poster the shortest shutter of 8.4 ns was used. A few shots were done with 50 ns shutters and are discussed later.

C. Dynamic Response

A computer records the output of the CID chip as a 752 by 480 matrix of 8-bit integers representing the intensity of each pixel of the CID chip. A value of 0 translates to no light being collected by that pixel. A value of 255 indicates that the pixel was saturated with light. Of the 256 intensity levels a pixel may have, most pixels in the captured images achieve an intensity level of less than 180. Therefore, the dynamic response of the camera was underutilized, and the camera was almost never saturated with light.

D. Sensitivity

The bias voltage applied to the multichannel plate controls the gain of the camera. For all the data taken for this poster, the maximum bias voltage was used to produce the maximum gain and, therefore, the most sensitivity to light. There exists a tradeoff between the time resolution and the sensitivity. Since the camera integrates the light over the time the shutter is open, a longer shutter will produce a greater sensitivity to light at a loss of time resolution. Figures 2 and 3 demonstrate trading time resolution for sensitivity.

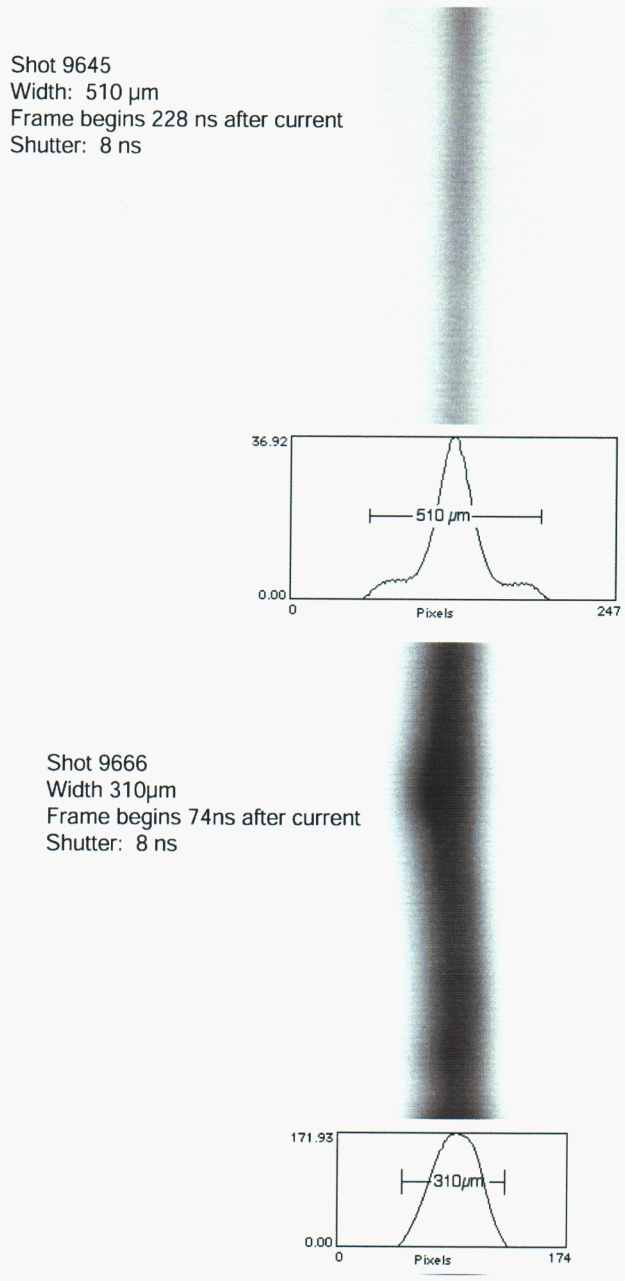

Figure 2. Example of framing camera pictures and intensity profiles.

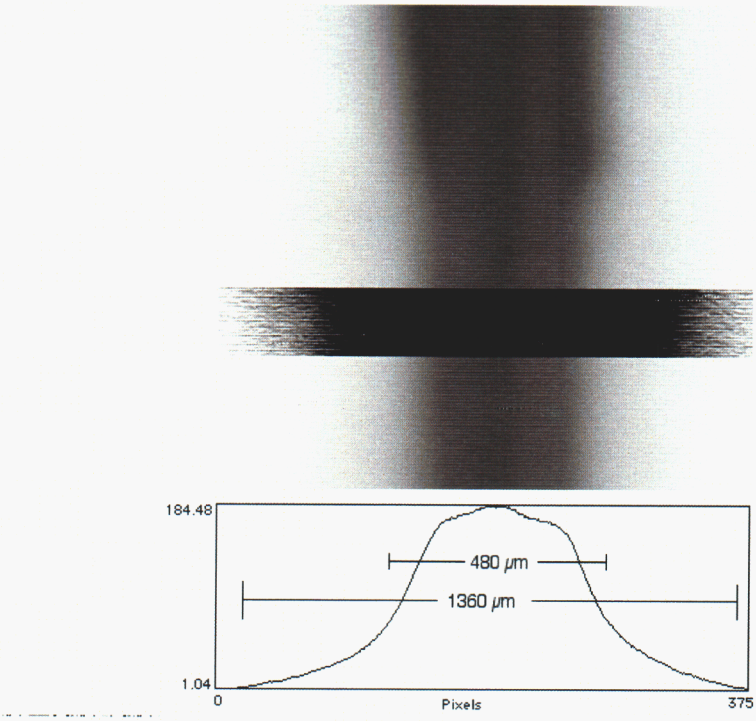

Shot 9686
Frame Begins 125 ns
after current starts
Shutter Width: 50 ns
25 µm Copper Wire

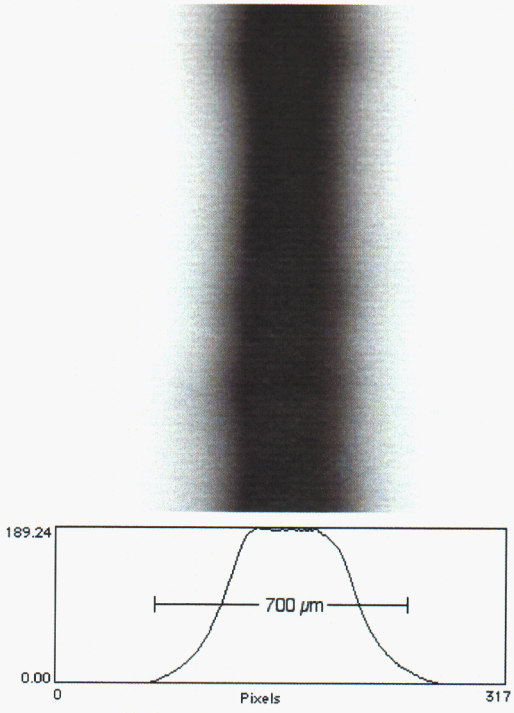

Shot 9689
Frame Begins 71 ns
after current starts
Shutter Width: 35 ns
25 µm Copper Wire

Figure 3. Examples of longer shutter times.

FRAMING CAMERA VERSUS LASER INTERFEROMETRY

The framing camera has a lower spatial and temporal resolution than laser interferometry being done at Cornell. The framing camera has a spatial resolution of 50 μm and takes pictures integrated over 8 ns. The laser interferometry is better by a factor of two in both categories. The interferometry uses a laser beam projected through the wire and plasma, so it will work for later times. The framing camera uses self radiation from the plasma, so as the plasma diminishes, so does quality of the framing camera pictures. Despite these drawbacks, the camera does have its advantages over the interferometry. At times close to voltage breakdown, the framing camera can see plasma nearly twice as far out as the interferometry illustrated in Figures 4 and 5. Around 200 ns after the current starts, the interferometry gives a better picture. The interferometry also shows a clear expansion of plasma. The framing camera suggests an expansion, but fails to definitely prove it.

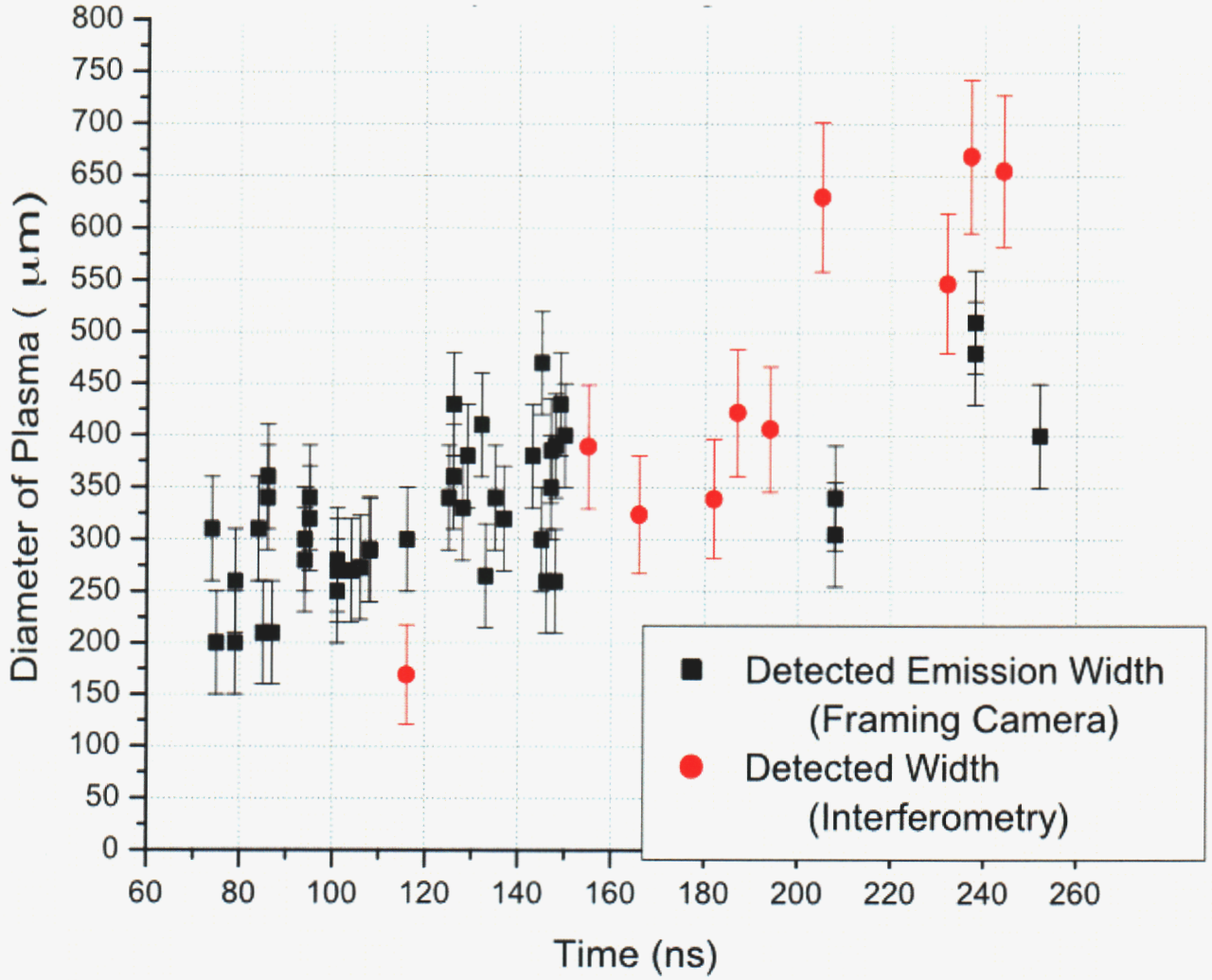

Figure 4. Comparison of framing camera and interferometry in measuring plasma width.

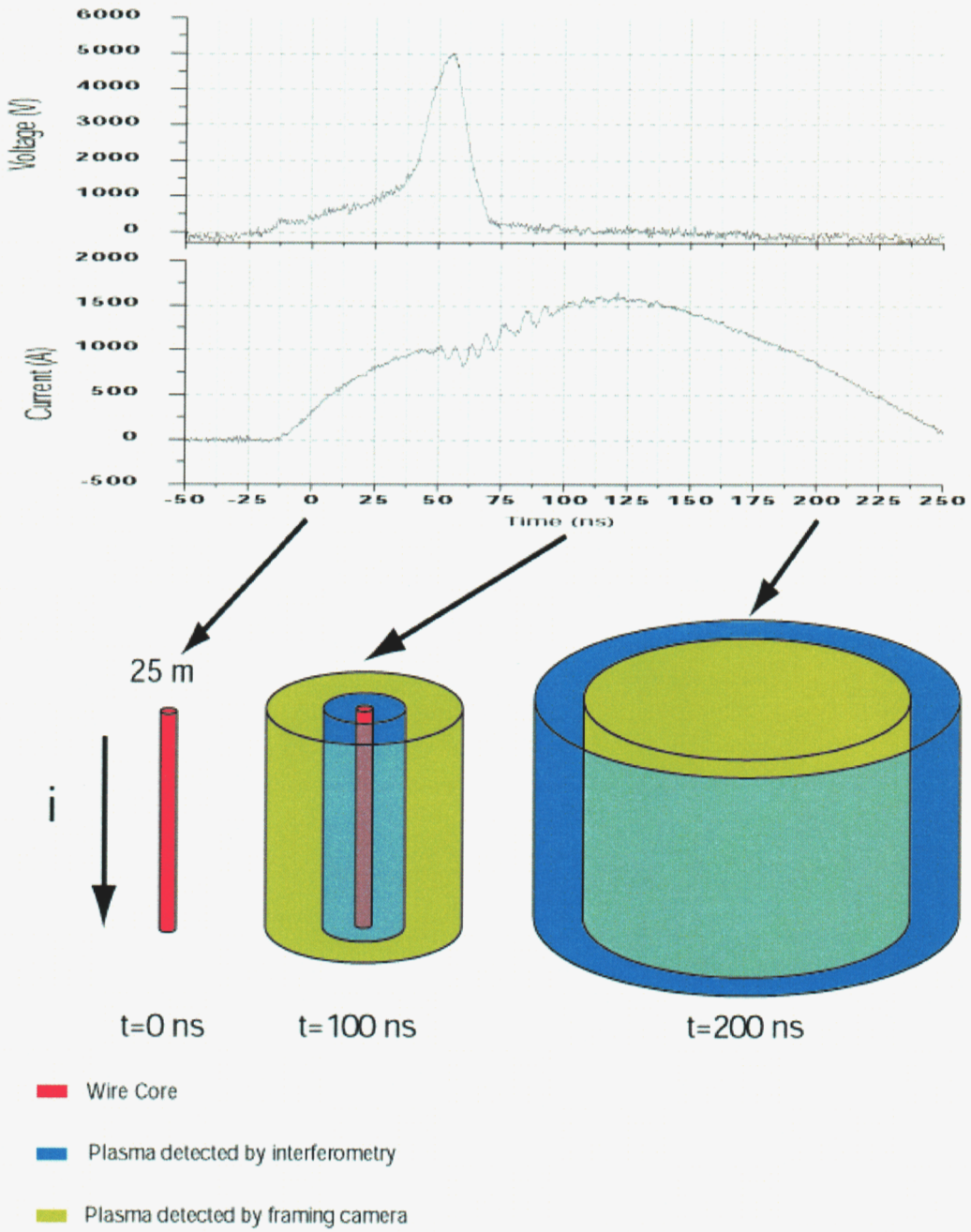

Figure 5. Typical voltage and current traces 1 cm of 24 μm copper wire.

EXPLAINING THE DRAMATIC DROP IN RESISTANCE OF A PULSED WIRE

A cable driven pulser drives a single 25 μm Copper wire with a rise time of 20 A/ns and duration of 100 ns. During this pulse, the wire goes through several phases as evidenced by Figure 6. During the time labeled Phase I, the current driven through the wire causes heating. Heating the wire increases the resistivity of the wire, and hence the voltage also increases. About 65 ns after the current starts, a dramatic change occurs (Phase II). During this time, the voltage drops dramatically two orders of magnitude from 5000 V to less than 100 V. The voltage displayed in Figure 6 has been corrected for the inductive voltage found in the system. The drop in resistance is attributed to the formation of plasma around the wire. At this time it is uncertain if the plasma is composed of metal ions or surface contaminants from the wire. Regardless, after the plasma forms, the measured resistance falls to less than 0.25 Ohms and the current is limited only by the impedance of the machine. This experiment shows that one can use reasonable measured values for plasma temperature and width to calculate a resistivity comparable to what is actually measured.

A framing camera was able to observe a 700 μm wide column of plasma around the wire within 35 ns after the voltage starts to collapse and 105 ns after the current starts. It is not unreasonable to assume a plasma expansion rate of 6.7 μm/ns and, therefore, a plasma width of 460 μm at the time of voltage collapse. The temperature of the plasma was taken to be 3 eV based on the expansion rate of the plasma and assumption that the plasma is composed of nothing lighter than carbon. Assuming a carbon composition can be justified given the likelihood of surface contaminants. More likely is the case where the plasma composed of heavier atoms or molecules and, therefore, much hotter then 3 eV. At voltage collapse, the Spitzer resistivity is:

$$\eta = 5.2\times10^{-5}\frac{Z\ln\Lambda}{T^{3/2}(eV)}\Omega\cdot m = 5.2\times10^{-5}\frac{1\cdot 8.2}{(3)^{3/2}}\Omega\cdot m = 8.1\times10^{-5}\Omega\cdot m$$

Hence, for the experimentally measured plasma width A and wire length L, the expected resistance is:

$$R = \frac{\eta L}{A} = \frac{(8.1\times10^{-5}\Omega\cdot m)(1cm)}{\pi\left(460\mu m/2\right)^2} = 4.8\Omega$$

The result is an order of magnitude too large. However, if one repeats these calculations assuming the plasma to be composed of copper, one gets that the resistance should be 0.44 Ω, the same order of magnitude as the observed value.

TRADING TIME RESOLUTION FOR SENSITIVITY

For this particular frame the shutter of the framing camera was lengthened from 8 ns to 50 ns. Since the camera integrates light over the duration of the shutter, it was able to see fainter plasma. For similar frames taken with fast 8 ns shutters, the plasma width is only around 400

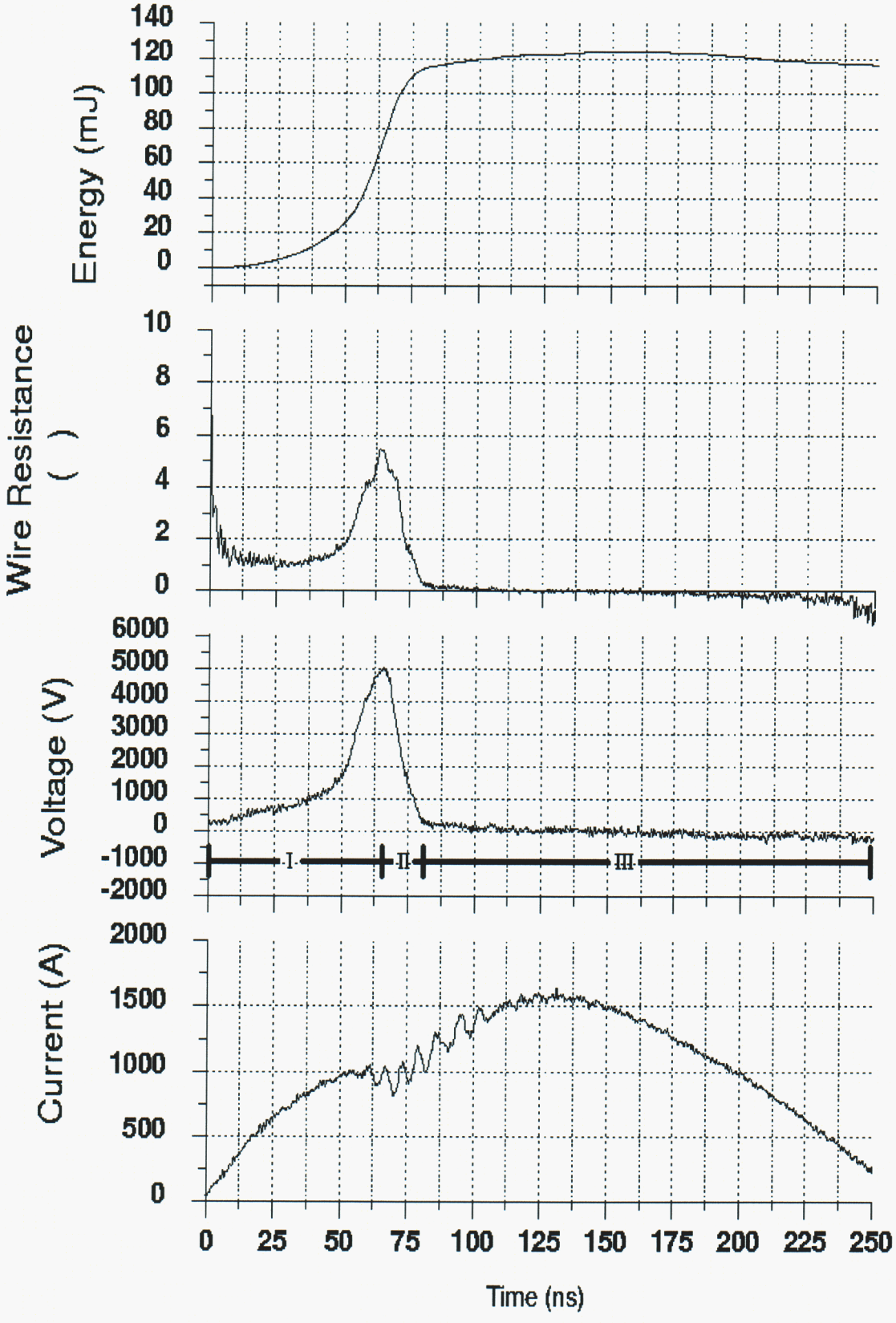

Figure 6. Typical electrical characteristics of a 1 cm long, 25 m copper wire.

μm. The tradeoff, illustrated by Figure 3, is that we lose most of the information about when the plasma is formed or how it is propagating. Another minor problem is that when the shutter length gets much more than 50 ns, the camera becomes too sensitive to light and saturates on the more intense parts of the pictures. Earlier, while calculating the resistivity of the detected plasma, an expansion rate was calculated. This rate was calculated using a frame with a longer than normal 35 ns shutter and the slowest expansion rate was used.

RULING OUT THE EXISTENCE OF PLASMA BEFORE VOLTAGE BREAKDOWN

In order to support the hypothesis that plasma formation causes voltage collapse, one needs to eliminate the possibility of plasma existing before the voltage collapse. The framing camera can detect the emission of light from the plasma formed around the wire, but a vacuum photo diode does it with a better sensitivity to light and time resolution. The diode employed in this experiment was a homemade diode constructed from a coax connector. It is illustrated in Figure 7. The photocathode was an aluminum foil disk with approximately 2 cm^2 exposed to light from the exploding wire. The anode is a mesh that is held at ground approximately 2 mm away from the photocathode. The diode itself was mounted approximately 10 cm from the wire with the photocathode negatively biased. The first few attempts to utilize this vacuum diode produced saturated signals as the voltage bias was not negative enough. At a bias of –900 V, the diode produced signals that showed no signs of distortion. This vacuum photo diode has a rise time of less then 1 ns.

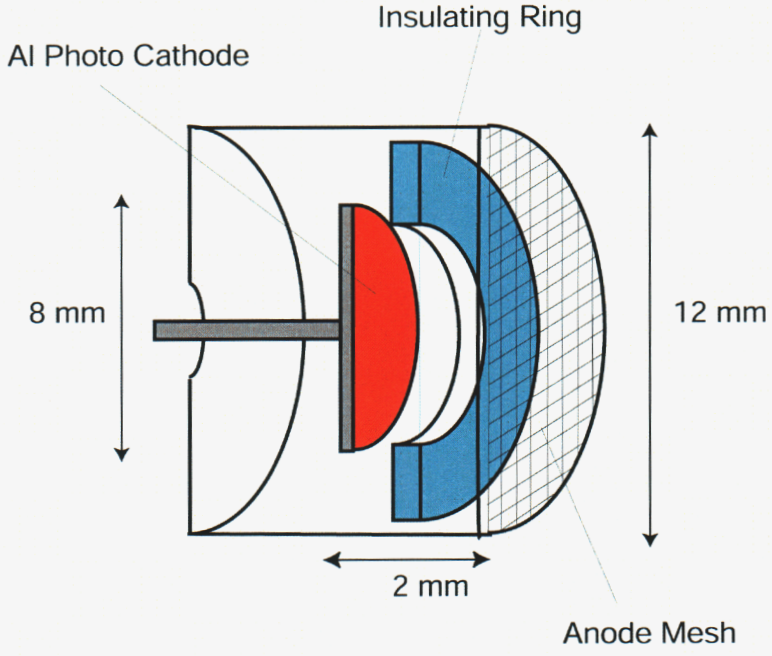

Figure 7. Vacuum photo diode.

The vacuum diode clearly shows that there is no light coming from the exploding wire until the voltage collapse (Figures 8 and 9). Thus, it is established that plasma is not formed earlier then expected. The remaining structure of the vacuum diode trace has some curious structure. The signal is very sharply peaked at voltage breakdown, indicating a large amount of light is radiated from the wire initially when the plasma is formed. As time progresses, the signal intensity decreases even though the current through the plasma is still increasing. At first glance one might suppose that the fall-off of signal should be attributed to some sort of decay time of the diode and its supporting circuitry. This idea is dismissed when one looks at the images produced by the framing camera. The framing camera also records light intensity. Although not nearly as sensitive as the diode, it sees peak pixel intensities 3 times greater immediately after the plasma forms than when the current peaks. The expanding plasma can lower the current density while increasing the total amount of current.

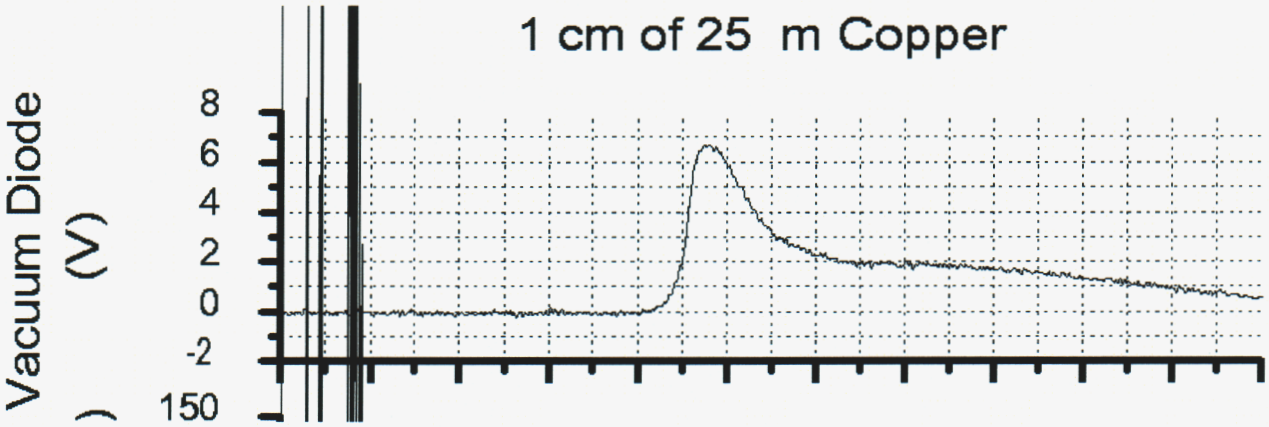

Figure 8

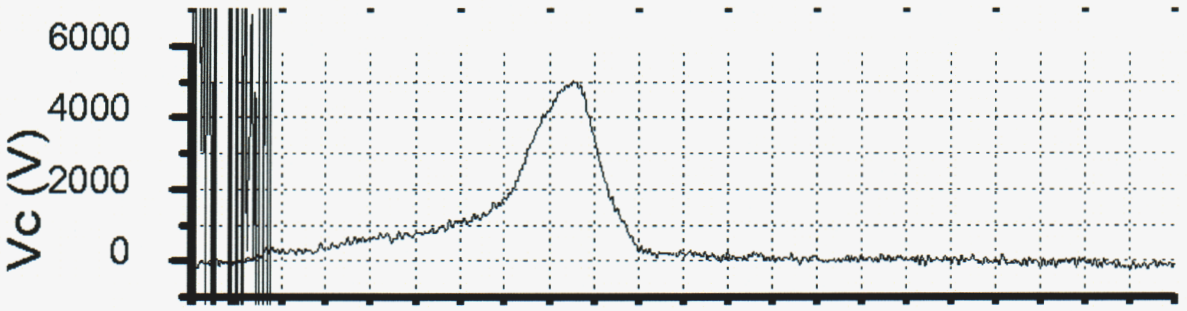

Figure 9

The topic of frequency spectrum was partially addressed in this experiment. When the diode is filtered by a piece of glass that does not pass UV, it does not produce a signal. This says more about the response of the diode than the radiation from the exploding wire. Because of the work function of aluminum, one naturally expects it to be more sensitive to UV than the visible light.

Conclusions

When we understand the connection between the initial conditions and the results of wire-array implosion experiments, choosing the best wires for specific wire-array z-pinch applications will be possible. For example, an alloy might be expected to have advantageous radiative properties for a particular application. The latter will be facilitated by computer simulations using codes that take their initial conditions from single wire experiments and then calculate the dynamics and radiative properties of wire array implosions, including the properties of those materials. First, however, it will be necessary to validate those codes, including the material equations-of-state and conductivity, against single-wire explosion experiments such as those reported here.

This research was supported by Sandia contract BD-9356 and DOE contract DE-FG03-98DP00712

APPENDIX

Experiments measuring the initial energy deposition, expansion rates and morphology of exploding wires with about 1 kA/wire

D. B. Sinars, Min Hu, K. M. Chandler, T. A. Shelkovenko,[a] S. A. Pikuz,[a]
J. B. Greenly, D. A. Hammer,[b] and B. R. Kusse
Laboratory of Plasma Studies, Cornell University, Ithaca, New York 14853

(Received 2 August 2000; accepted 11 September 2000)

Wire-array Z-pinch implosion experiments begin with wire heating, explosion, and plasma formation phases that are driven by an initial 50–100 ns, 0–1 kA/wire portion of the current pulse. This paper presents expansion rates for the dense, exploding wire cores for several wire materials under these conditions, with and without insulating coatings, and shows that these rates are related to the energy deposition prior to plasma formation around the wire. The most rapid and uniform expansion occurs for wires in which the initial energy deposition is a substantial fraction of the energy required to completely vaporize the wire. Conversely, wire materials with less energy deposition relative to the vaporization energy show complex internal structure and the slowest, most nonuniform expansion. This paper also presents calibrated radial density profiles for some Ag wire explosions, and structural details present in some wire explosions, such as foam-like appearance, stratified layers and gaps. © *2001 American Institute of Physics.* [DOI: 10.1063/1.1323759]

I. INTRODUCTION

Z-pinch implosions with extremely high energy densities have recently been achieved on the Z-machine[1] at Sandia National Laboratories, Albuquerque, using cylindrical arrays of fine wires.[2–4] The success of the wire-array Z-pinch program has stimulated interest in their use as x-ray sources for inertial confinement fusion,[5–7] studies of astrophysical jetting phenomena,[8] and studies of material properties under extreme conditions.[9] The implosion phase in these wire-array Z-pinch experiments is preceded by wire heating, explosion, and plasma formation initiated by a 50–100 ns, 0–1 kA per wire current ramp ("prepulse"). Similarly, in 64-wire array experiments on the MAGPIE[10] generator at Imperial College, the current rises from 0 to 1 kA per wire in about 40 ns.[11] There is great interest in understanding the initial stages of wire explosions starting from the cold wire state because those explosions provide the initial conditions for the implosion dynamics of wire arrays.

Studies of the effect of prepulse-like conditions on the explosion of 1–3 wires[12–14] showed that the wire expansion rate and uniformity was strongly dependent upon the amount of energy deposited in the wires during a short (<100 ns) resistive heating phase. This resistive phase is terminated by a sudden collapse of the voltage across the wire, probably due to plasma formation. Recent experiments demonstrated that it was possible to prolong the resistive heating phase of 25 μm diameter W and 25 μm diameter Ag wires through the use of thin insulating coatings on the wires.[14] The additional energy that was deposited in the wires with insulation resulted in substantial increases in the observed expansion rates of the dense wire cores.

The experiments described here investigated the current-driven explosions of several different wire materials, including Al, Ti, Fe, Cu, Zn, Nb, Mo, Ag, W, Au, and Pt. The effect of insulating coatings on the rate and uniformity of expansion of individual 25 μm diameter Ag, Cu, and W is also presented, including more data than previously reported for Ag and W.[14] The key parameter appears to be the energy deposited in a wire relative to the total energy required to vaporize it. Tungsten was a major element in this study because it is a commonly used wire material in wire array Z-pinches. This is because it can easily be drawn into wires as small as 4 μm in diameter, has a high tensile strength, and is desirable for x-ray production in the keV range. However, our initial work demonstrated that the resistive energy typically deposited in W wires is a small fraction of the energy required to completely vaporize the wire. Consequently, relatively slow and nonuniform expansion was observed. By contrast, the energy resistively deposited in Ag wires is nearly that required to completely vaporize the wire, and relatively fast and uniform expansion is observed. We, therefore, included Ag wire experiments as a major element in this study because they offered such a contrast to W. In addition, as an intermediate Z material, Ag is well matched to our radiographic backlighting diagnostic. Relatively early in the explosion process enough x-rays are transmitted through the core to allow quantitative density measurements, and later in the explosion development, when the core has expanded to more than 50 times its original diameter, most of the initial mass is still resolvable by the x-rays.

As a general rule, among the many materials tested so far, high-conductivity, low melting-point materials form more uniform, rapidly expanding columns of wire material. Thus, the core dynamics of W, Pt, Mo, and Ti wires are quite

[a]Permanent address: P. N. Lebedev Physical Institute, Moscow 117924, Russia.
[b]Also at School of Electrical and Computer Engineering, Cornell University, Ithaca, NY 14853.

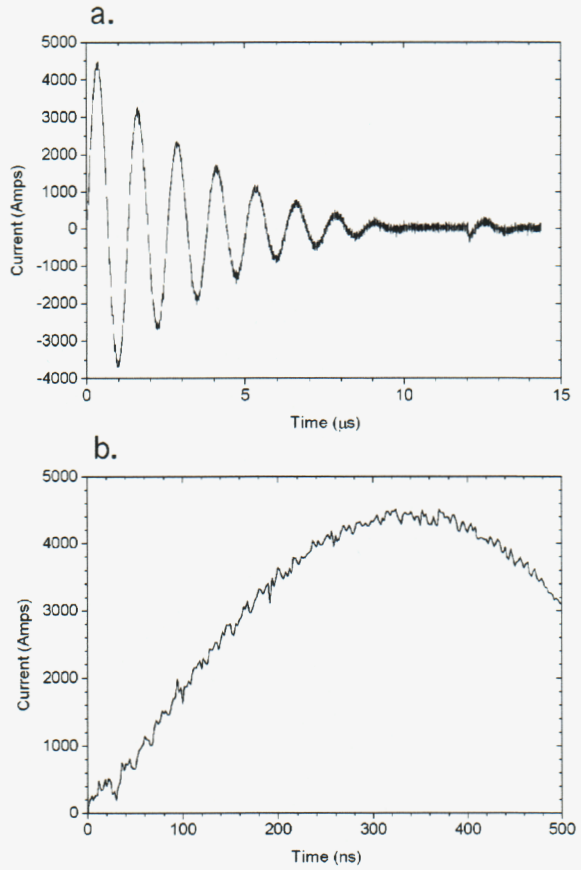

FIG. 1. Current waveform delivered to a low-inductance and low-resistance load by the LC1 pulser. The full damped waveform is shown in (a), while (b) shows the first 500 ns of the pulse.

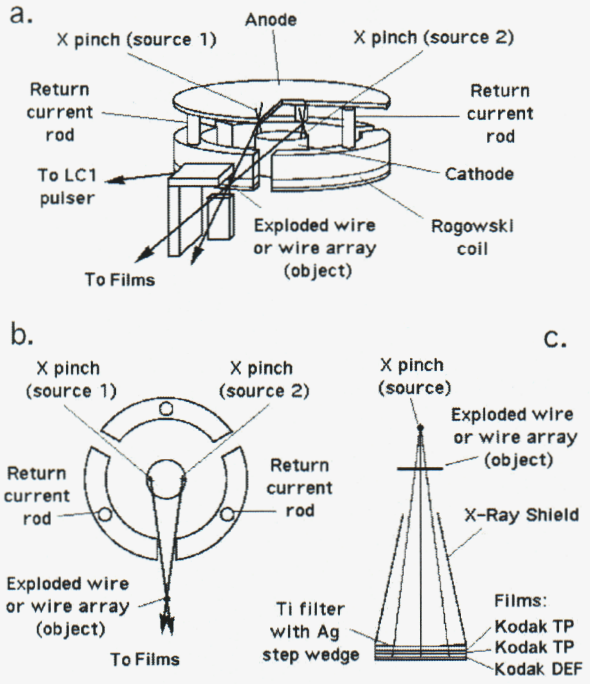

FIG. 2. Schematic diagram of the experimental arrangement. (a) The XP pulser load region with two X pinches and its relationship to the exploding wire or wire array (object) powered by the LC1 pulser. (b) A top view of the X-pinch backlighters and the object. (c) The backlighter–wire/wire array–x-ray film arrangement. The backlighter-to-wire distance was about 7.9 cm, and the backlighter-to-film distance was about 33 cm.

different from the core dynamics of Al, Cu, Ag, and Au wires, and we can classify most materials as belonging to one group or the other. Furthermore, we find that insulating coatings prolong the resistive heating phase for wires in both groups of materials, thereby increasing the wire core expansion rates. The database that is provided in this paper should be useful for the validation of computer codes that are presently being developed to carry out wire explosion simulations from a cold start.[15–17]

The remainder of this article begins with a description of the experimental system used to determine the behavior of the cores in current-driven wire explosions. Results and discussion follow in Sec. III. In Sec. IV, we present conclusions, including a discussion of some of the experiments that are still needed.

II. EXPERIMENT DESCRIPTION

The majority of the experiments described here involved 1-cm long, 7.5–25 μm diameter wires driven by a 4.5 kA peak current pulser. Eleven different wire materials were tested, including Ag, W, and Cu, which were tested both with and without an insulating coating. The current was supplied by the LC1 pulser, which consisted of a low-inductance 75-nF capacitor charged to about 15 kV. When driving a low-inductance, short-circuit load, this pulser produced a damped sinusoidal current pulse having a 350 ns quarter period rise time, an amplitude of 4.5 kA, and an e-fold damping time of 4.25 μs, as shown in Fig. 1. When wire loads were used, a shunt monitor located at the wire measured the wire current, and a resistive voltage monitor measured the voltage across the wire. All of the wire experiments reported here were carried out at a pressure of $<1\times10^{-4}$ Torr.

Radiographs of the wire explosions were made as functions of time relative to the start of the LC1 current pulse using Mo X pinches as direct x-ray backlighters.[18] With an appropriate current pulse, Mo X pinches typically produced 1 (sometimes 2) intense x-ray bursts in the 2.5–10 keV range with pulse durations <0.25 ns.[19] A single radiographic image with a spatial resolution of 2-5 μm was obtained from each burst using direct x-ray backlighting.[19] (If two equally intense bursts were produced from the same X pinch, a noticeable "double-image" was obtained on the film.) The spatial resolution in each radiograph was determined by the quality of its backlighter X pinch and the diffraction limit for the x-rays used to expose the film. By using one X pinch composed of 17 μm diameter Mo wires and one composed of 30 μm Mo wires, two separate radiographs of one wire explosion were made up to 30 ns apart. The radiographs were recorded on three x-ray sensitive films in series in a shielded camera behind a 12.5 μm Ti filter. Figures 2(a) and 2(b) show the experimental setup used to obtain the radio-

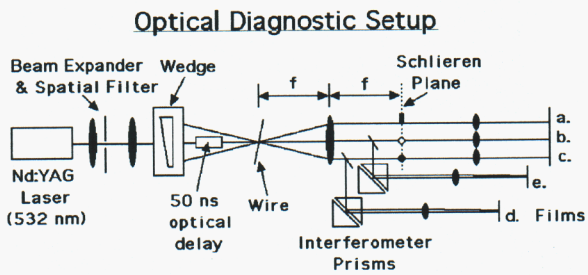

FIG. 3. Schematic diagram of the Nd:YAG laser optical system setup. The second harmonic of the Nd:YAG laser beam (532 nm) passes through a spatial mode filter, is expanded to 3 cm × 1.5 cm, and then is split into three separate beams using a wedge. One beam is optically delayed by 50 ns, and all three beams pass through the experiment chamber with an angular separation of approximately 1.43°. Two of the three beams are split again to send a portion through air-wedge shearing interferometers. All three remaining beams are used to generate schlieren images. The films are classified as follows: (a) dark-field knife-edge schlieren channel, (b) bright-field iris schlieren channel (50 ns delayed), (c) dark-field strip schlieren channel, (d) first interferometry channel, and (e) second (50-ns delayed) interferometry channel.

graphs, which typically had a magnification of about 4.2:1. Figure 2(c) shows the film and filter arrangement in the camera. The radiographic films, Kodak Technical Pan (TP) (similar to Kodak RAR 2497) and Kodak DEF, were scanned using a 4000 dpi Polaroid SprintScan scanner.

The current for the two parallel X pinches was supplied by the 450 kA, 100 ns pulse duration (40 ns 10%–90%rise time) XP pulsed power generator.[20] The x-ray radiation bursts produced by the X pinches were recorded using fast diamond photoconducting detectors (PCDs) and a 5 GS/s Tektronix 684B digitizing oscilloscope. The relative timing of the x-ray bursts and the start of the LC1 current pulse was determined to within ±2 ns.

Schlieren and interferometry images were also recorded as functions of time using a 4 ns pulse at the second harmonic of a Nd:YAG laser (λ=532 nm, plasma cutoff density $=4\times10^{21}$ cm^{-3}). A schematic diagram of the optical system setup is shown in Fig. 3. The interferometry was carried out with novel, air-wedge, shearing interferometers, which are described in detail elsewhere.[21] The pulse was split into multiple beamlines, some of which were optically delayed to obtain images of one wire explosion at times up to 50 ns apart. The laser images were recorded on Ilford HP5 400 film, and the films were scanned using a 2700 dpi Nikon LS-2000 scanner. The diffraction-limited spatial resolution of the schlieren images was about 20 μm.

When we compared optical interferometry images of greatly expanded insulated Ag wires with and without x-ray backlighting, we found an increase in the amount of plasma generated immediately adjacent to the wire core in pulses with the backlighting compared to pulses without the backlighting. A few experiments determined that UV (ultraviolet) radiation from the XP pulser diode near the time of the x-ray bursts was probably responsible for the increase of plasma. The UV radiation's effects can be eliminated through the use of an appropriate filter to stop UV while allowing the 2.5–10 keV x-rays through. Practically speaking, however, the additional plasma had no effect on any of the measurements presented in this paper.

Two types of wires were used in these experiments, bare wires and manufacturer-insulated wires with a known thickness of plastic. The insulated 25 μm W wires had a 5 μm coating of polyimide, the insulated 25 μm Ag wires had either a 1 or a 5 μm coating of polyester, and the 25 μm Cu wires had a 5 μm coating of polyurethane. All of the wires studied are commercially available. In our initial studies on the effect of insulating coatings,[14] we also used oil coatings applied to the wires, but these studies were not continued due to concerns over the uniformity and reproducibility of the oil coatings.

By testing 25 μm Ag wire with two different thicknesses of insulation, 1 μm and 5 μm, we intended to determine the effect of the insulator thickness on the breakdown characteristics. Possible advantages to having a thicker layer of insulation are an increased delay in the formation of plasma around the wire relative to that found with 1 μm polyester[14] and a greater tensile strength of the wire plus coating with little additional mass. The increased strength is necessary if wires made of "soft" metals, such as Ag or Au, are to be used in wire-array experiments. Attempts to use Au wires on the Z-machine at Sandia were unsuccessful because the wires stretched or broke when held in place by weights in a multiwire array and had a greater tendency to kink during handling.[22] Possible problems resulting from the use of thicker insulating layers include making a satisfactory initial contact between the wire and the LC1 pulser load electrodes, increased nonuniformity in the wire expansion if the insulator breakup is uneven, and adverse effects on the wire-array Z-pinch implosions due to the additional plastic.

In our experiments, a 1-gram weight was typically used to keep the wires straight. If used with a 25 μm diameter wire, the wire experiences a tension of about 16 MPa. The ultimate tensile strength of Ag is 140 MPa, and the tensile yield strength of polyester is about 55 MPa. Since we typically used 25 μm wires, wire stretching was not a problem in our experiments. Wire-array Z-pinch experiments, by contrast, often use much smaller wires, such as 7.5 μm W. Using a 1-gram weight with a 7.5 μm W wire implies a tension of about 180 MPa, which does not pose a problem since the tensile yield strength for W is 450 MPa. If, however, the 7.5 μm W wire is replaced by a 7.5 μm Au wire (which has the same mass), the ultimate tensile strength of Au (120 MPa) would be exceeded. However, by coating the 7.5 μm Au wire with a 2.5 μm coating of polyimide, which has a tensile yield strength of about 120 MPa, the tension can be reduced to about 65 Mpa. This estimate assumes that the polyimide and Au support the 1-gram weight in proportion to their cross-sectional areas.

Previous experiments using 25 μm Ag wires with a 1 μm polyester coating indicated that initial electrical contact did not seem to be a problem. By contrast, similar tests using a 5 μm polyimide coating on 25 μm W wires showed that the initial electrical contact was very poor, resulting in expansion only near the cathode end of the wire.[14]

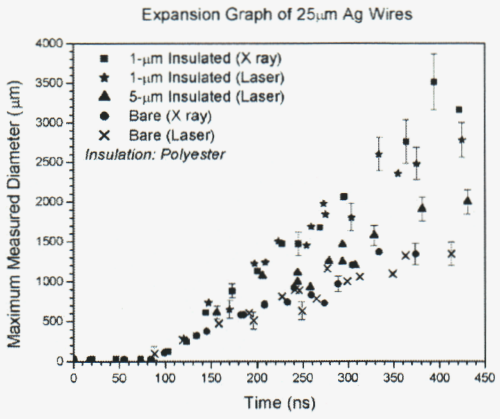

FIG. 4. Graph of the maximum measured wire core diameter versus time for bare 25 μm Ag wires and 25 μm Ag wires with polyester insulating coatings. Data points from radiographs and interferograms are shown.

III. RESULTS AND DISCUSSION

We begin our presentation of results with 25 μm Ag wire experiments. These were tested bare and with 1- or 5-μm thick coatings of polyester. No special precautions to ensure initial electrical contact were taken with the coated Ag wires. Figure 4 presents a graph of the maximum visible wire core diameter versus time for 22 tests. The graph in Fig. 4 combines data from two different diagnostics: the x-ray backlighting images (often two points separated by 15–30 ns per pulse) and the laser interferometry images (two points separated by 50 ns for most of the pulses). In the case of x-ray backlighting, the diameter of the wires was measured by scanning the images into a computer and plotting the optical density profile to determine the full width of the wire core profile. In the case of laser interferometry images, the plasma–neutral boundary was chosen as the outside edge of the wire core. (More precisely, we used the point of zero net fringe-shift between the negative refractive index shift caused by the plasma and the positive shift caused by the neutral metal vapor.) Due to the large number of different data points on this plot, example error bars are included for only a few of the points. The error bars for the radiograph and interferometry points include the difficulty of resolving the boundary of the expanded wire, which becomes progressively more difficult as the wire expands. The error bars for the interferometry points include an adjustment for the minimum spatial resolution of the diagnostic. As the series of x-ray backlighting images in Figs. 5 and 6 show, the expansion of Ag wires (coated or bare) was normally reasonably uniform axially, at least on the mm scale. Thus, the maximum visible diameter is a simple, representative indicator of the overall wire expansion at each time. Because at most two x-ray backlighting and two laser interferometry images were obtained from a single wire test, the points in this graph represent data from a large number of exploding wire experiments. The time of each image is stated relative to the start of current flow in the test wire. The stratification (small-scale axial nonuniformity) of the exploding wires visible in all of the Ag radiographs will be discussed shortly.

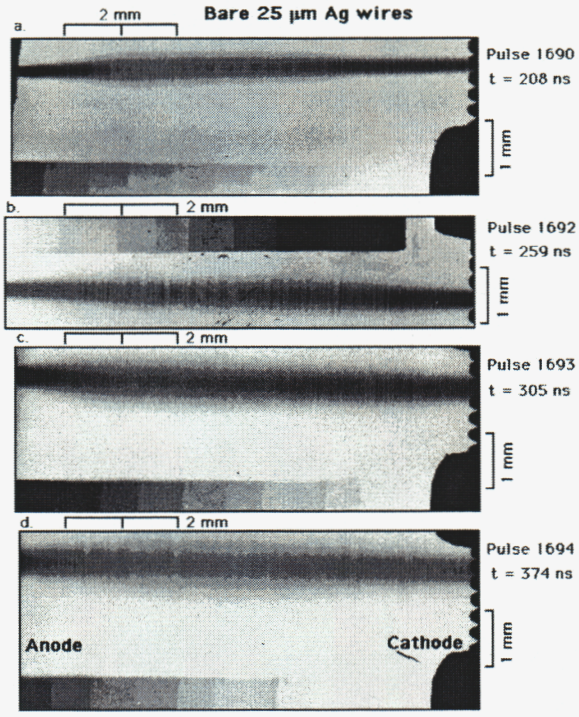

FIG. 5. X-ray radiographs of exploding, bare 25 μm Ag wires. The times given are relative to the start of the current flow in the wire: (a) 208 ns, (b) 259 ns, (c) 305 ns, and (d) 374 ns. Each radiograph is from a different test pulse, and it includes an image of the Ag step wedge for the calibration of areal mass density measurements. The step wedge thickness values, from thinnest to thickest, are 0.05, 0.10, 0.20, 0.30, 0.40, 0.60, 0.80, 1.20, 1.59, and 1.80 μm.

A clear difference in wire expansion between 1 μm insulated and bare 25 μm wires is seen in Fig. 4. However, Ag wires insulated with a 5 μm polyester layer expanded only marginally faster than the bare wires. A second feature visible in Fig. 4 is that the expansion of the wire cores does not begin immediately with the start of current flow in the wire. The expansion of bare Ag wires appears to begin 65–70 ns after the start of current flow, whereas the expansion of 1 μm polyester-insulated 25 μm Ag wires begins perhaps 10–20 ns later. Thus, to obtain an average linear expansion rate for the wire core diameter, only data in Fig. 4 after the start of core expansion were fitted, taking into account the error in each measurement. The results of these fits are shown in Table I.

The time delay before the start of expansion in Fig. 4 can be understood from the wire current and voltage during the first 100 ns of the current pulse. Sample waveforms of the current and voltage for bare, 1 μm insulated, and 5 μm insulated 25 μm Ag wires are plotted in Fig. 7, as is the estimated energy deposited in the wire cores calculated by integrating the current–voltage product. The inductive contribution to the voltage is estimated to be less than 500 V at the peak voltage of about 32 kV, so no inductive correction has been made to the measured wire voltage. The wave-

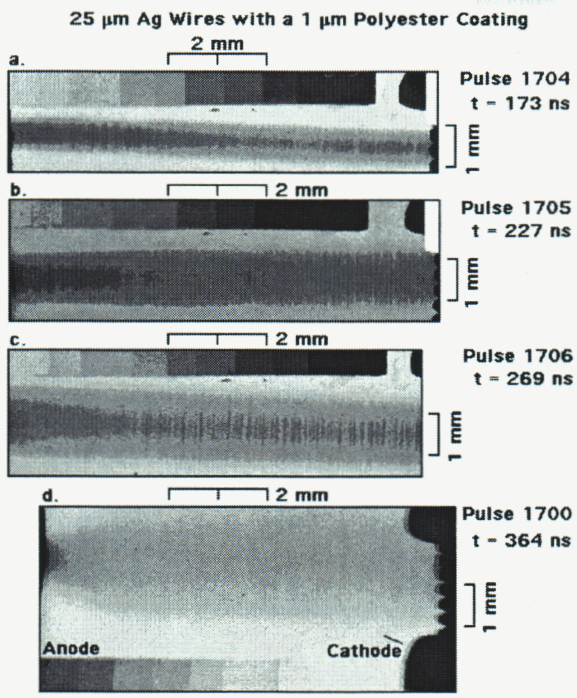

FIG. 6. X-ray radiographs of exploding 25 μm Ag wires coated with 1 μm of polyester insulation. The times given are relative to the start of the current flow in the wire: (a) 173 ns, (b) 227 ns, (c) 269 ns, and (d) 364 ns. Each radiograph is from a different test pulse, and it includes an image of the Ag step wedge (see the Fig. 5 caption for details). Note that the image in (d) is a "double exposure" caused by two x-ray bursts from a single X pinch.

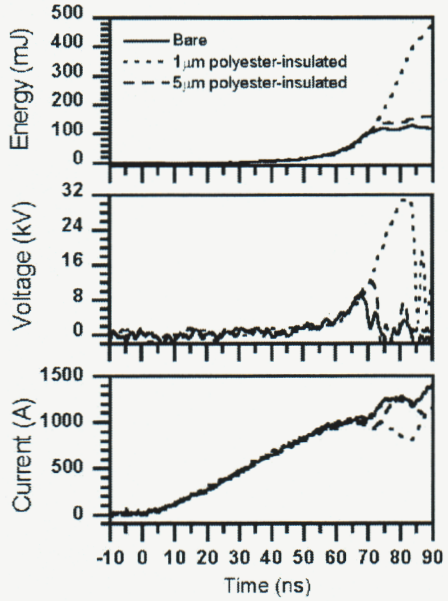

FIG. 7. The first 90 ns of the current and voltage applied to 25 μm Ag wires by the LC1 pulser, and the energy deposited in the wire. The three cases shown are bare, 1 μm polyester-insulated, and 5 μm polyester-insulated 25 μm Ag wires.

forms plotted in Fig. 7 are typical results obtained using each type of wire.

The voltage and current waveforms indicate that the wires experience a short, resistive heating phase that is terminated by a rapid collapse in the voltage. The voltage along a silver wire is quite low initially, increasing significantly only as the wire material is heated and becomes more resistive. The resistance of a 1-cm long, 25 μm diameter Ag wire rises from about 0.4 Ω at room temperature to about 4.3 Ω at 1700 K.[23] For the waveforms shown in Fig. 7, the peak resistance measured is about 8 Ω for the bare 25 μm Ag wire and about 38 Ω for the 1 μm polyester-insulated 25 μm Ag wire. The peak voltage exceeded the charging voltage on the LC1 capacitor (about 15 kV) in the case of 1 μm insulated Ag because the inductance of the driving circuit, which is much larger than the inductance of the 1 cm long test wire, keeps current flowing through the wire as the wire resistance rapidly increases. Notice that the derivative of the current turned negative at the same time as the wire voltage exceeded the capacitor voltage. The time of voltage collapse (and the termination of the resistive heating phase) is defined here as the time at which the derivative of the current shows a sharp discontinuity in the positive direction, indicating a sudden drop in the load resistance. The initial resistive heating phase lasted about 70 ns for bare 25 μm Ag wires, about 85 ns for 1 μm insulated wires, and about 72 ns for 5 μm insulated wires for the tests shown in Fig. 7. Thus, the effect of the insulation was to prolong the resistive heating phase, resulting in a higher peak voltage and more energy deposition.

TABLE I. A summary of the fitted wire core diameter expansion rates for 25 μm Ag wires, either bare or polyester-insulated. The radiographic and interferometric data were analyzed independently and are presented as separate entries. Since the wires are not observed to expand prior to the time of voltage collapse, only data taken after this time were fitted.

Wire type	Fitted linear slope (μm/ns) and error
Bare 25 μm Ag (radiograph)	4.5±0.4
Bare 25 μm Ag (interferometry)	3.7±0.3
1 μm insulated 25 μm Ag (radiography)	10.3±0.5
1 μm insulated 25 μm Ag (interferometry)	8.2±0.6
5 μm insulated 25 μm Ag (interferometry)	5.1±0.6

We attribute the collapse of the voltage to the formation of plasma around the wire, with the plasma resistance quickly becoming much lower than the resistance of the heated wire core material. The plasma is believed to be formed from gases desorbed from the wire surface and/or from evaporated wire material as a result of breakdown driven by the electric field that is present close to the wire. However, in single-wire experiments at 0–1 kA per wire, this plasma is not visible in our interferograms. After plasma formation, virtually all of the current is shunted through plasma surrounding the residual wire core and the load voltage collapses. Thus, the wire core mass is directly heated only to a small extent after this time. The current after the voltage collapse matches that seen when the LC1 pulser has

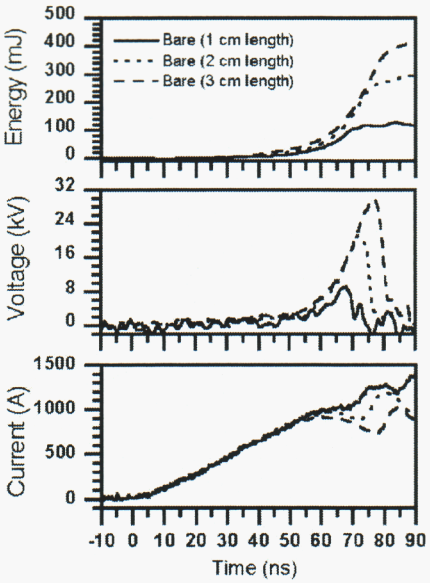

FIG. 8. The first 90 ns of the current and voltage applied to bare 25 μm Ag wires by the LC1 pulser, and the energy deposited in the wires. The three cases shown are 1-, 2-, and 3-cm long wires.

a short-circuit load (as shown in Fig. 2), and the load voltage remains essentially zero.

The energy required to fully liquefy a 1-cm long, 25 μm diameter Ag wire is estimated to be 20 mJ.[24] To fully vaporize the same wire requires a total of 138 mJ. In bare Ag wire experiments, the measured energy deposition in 9 tests was 108 ± 12 mJ. For 1 and 5 μm insulated Ag wire experiments, the measured energy depositions were 366 ± 32 mJ (13 tests) and 131 ± 17 mJ (7 tests), respectively. Thus, we expect that the Ag wire cores were largely vaporized, especially the 1 μm insulated wire cores. However, we note that this statement is quantitatively imprecise because we have not accounted for the considerable kinetic energy represented by the expansion speed of the wire core. Assuming a parabolic radial density profile and a linearly increasing radial velocity profile, we estimate the kinetic energy to be about 40 mJ in bare 25 μm Ag wire explosions.

Returning to Fig. 4, we note first that the expansion rates inferred for the three types of Ag wires plotted in Fig. 4 directly correlate with the measured energy depositions for each wire type. Second, the start times of the observed expansion in the cases of bare and 1 μm coated Ag wires appear to match the time of voltage collapse very well. The majority of the energy deposition occurs during the final 10–25 ns prior to the voltage collapse, as is evident in Fig. 7. During this time, the wire material likely undergoes two rapid phase transitions from solid to liquid and then from liquid to vapor. It is reasonable to expect that the wire would not expand visibly until this time. With Ag, the rapid expansion and ionization of metal vapor outside the dense wire core is believed to be responsible for triggering the voltage collapse, although adsorbed gases and hydrocarbon contaminants that desorb as the wire heats could play a role.

A short sequence of experiments was carried out to

TABLE II. A comparison of results from bare 25 μm Ag wires of different lengths. The electric field along the wire at the moment of breakdown and the energy deposition per unit length in the wire were nearly invariant with wire length.

25 μm Ag wire length	Time of collapse	Voltage at collapse	Energy at collapse
1 cm	69 ns	8 kV	100 mJ
2 cm	73 ns	20 kV	210 mJ
3 cm	78 ns	30 kV	310 mJ

study bare 25 μm Ag wires of 1-, 2-, and 3-cm lengths. Graphs of the current, voltage, and energy deposition waveforms for these experiments are plotted in Fig. 8. Examining the current waveforms for each wire length, we find voltage collapse times of about 69, 73, and 78 ns for the 1-, 2-, and 3-cm long wires, respectively. The voltages and energies at these times are listed in Table II. Both the electric field along the wires at the time of voltage collapse and the energy deposition per unit length in the wires were nearly invariant with wire length. Thus, the voltage collapse mechanism may be initiated at a critical value of either or both of these parameters.

Although we suspect that the 5 μm insulated Ag wires absorbed less energy than the 1 μm insulated wires because of poor initial electrical contact, mechanical methods to strip the insulation from the wires at the contact points were unsuccessful. Unfortunately, the softness and low melting point of Ag prevented us from scraping or burning the insulation off the wires. In future experiments, we will look for effective chemical means to remove the plastic. However, as we

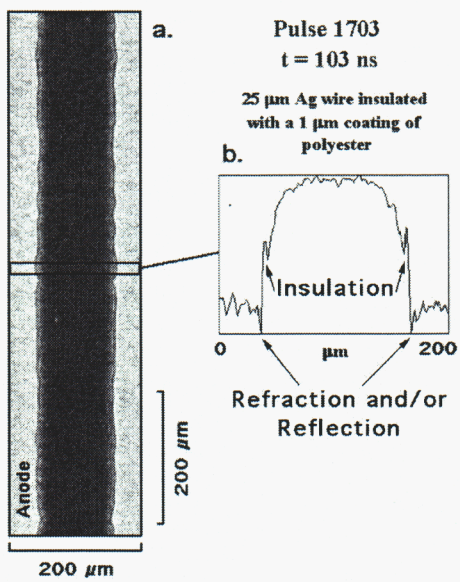

FIG. 9. (a) Radiograph of an exploding 25 μm Ag wire insulated with 1 μm of polyester taken 103 ns after the start of current, i.e., about 20 ns after the wire began to expand. Note the presence of cylindrically symmetric perturbations on the wire core. (b) A film density profile across the image averaged over a vertical height of ~20 μm, as indicated by the boxed region in (a).

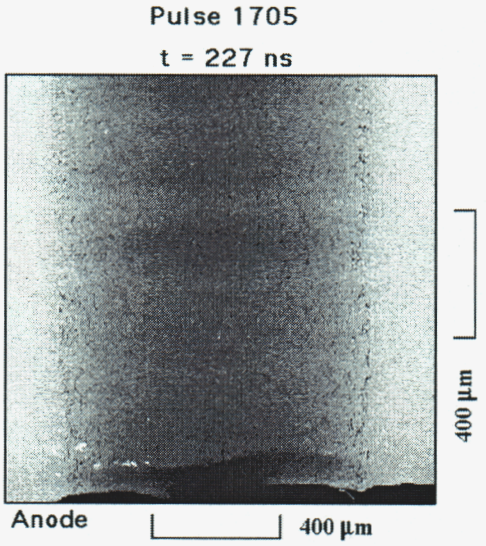

FIG. 10. Radiograph of the anode end of an exploding, 1 μm polyester-insulated 25 μm Ag wire at $t=227$ ns. Note the presence of fine, string-like particles of the solid insulation on the outside of the expanded wire.

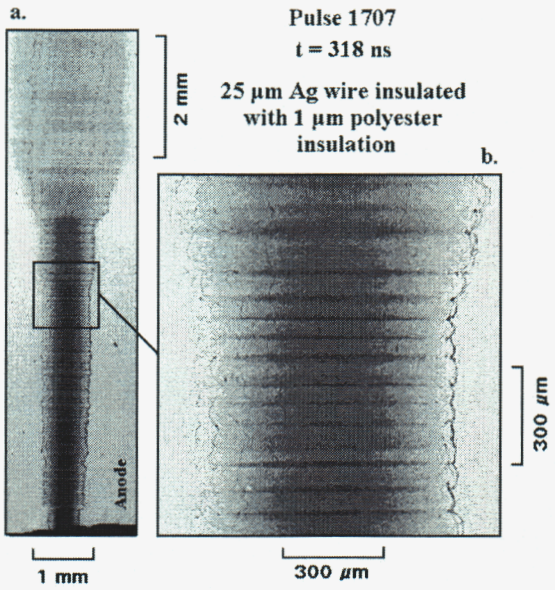

FIG. 11. (a) Radiograph of an exploding, 1 μm polyester-insulated 25 μm Ag wire taken at $t=318$ ns, the only wire of this type in 14 pulses to exhibit long scale-length axial nonuniformity. (b) An expanded view of the central region. Note the correlation between the periodicity of the insulation structure along the outside of the expanding wire and that of the stratification in the wire core. String-like bits of the insulation are visible also in front and/or in back of the expanding wire core.

noted in our previous publication,[14] the effects of a poor initial electrical contact with the electrodes were directly observable with W wires using both imaging and electrical diagnostics, and this will be reinforced shortly in our presentation of new W wire results.

The influence of the insulating layers on the expansion of the Ag wires following the voltage collapse is shown in a series of radiographs of tests at different times. Figure 9(a) shows an expanded view of a 25 μm Ag wire insulated with 1 μm of polyester from pulse 1703, at 103 ns after the start of the current, or approximately 15–20 ns after the voltage collapse. At this time, the measured wire diameter is about 125 μm, but the wire is not sufficiently expanded for the x-rays to penetrate the dense wire core. Small, cylindrically symmetric perturbations are visible in the boundary of the wire core. The film density profile shown in Fig. 9(b) indicates an outer shell surrounding the wire, which is presumed to be the insulating layer being pushed outward by the expansion of the Ag vapor (and/or contaminants).

Figure 10 shows an image of the anode end of the same type of wire at 225 ns after the current start (about 140 ns after the voltage collapse). The wire has expanded to a diameter of approximately 1 mm. This image shows thin strands of dense material all around the image of the wire core. The concentration of the material appears to increase toward the left and right edges of the wire core in the image, which suggests that the strands are concentrated in a thin radial layer surrounding the core. Similar structures appear in all 1 μm insulated 25 μm Ag wire explosions even at much later times, but never in bare 25 μm Ag wire explosions. We conclude that the structures are remnants of the insulation. Because the insulation conducts negligible current at room temperature (its resistivity is about 10^{21} times that of Ag), there should be virtually no resistive energy deposition in the insulating layer. The low solid density of the insulation (1.3 g/cm^3) assures us that if the polyester had been vaporized it would not be visible to the x-ray backlighting, allowing us to infer that the visible pieces are still condensed matter density. Thus, thermal conduction from the Ag to the plastic is evidently negligible on the sub-μs time scale, consistent with the thermal conductivity of polyester.

One recurring feature of coated and bare Ag wire explosions is the presence of stratified layers in the exploding wires. This stratification persists for hundreds of ns, and is remarkably planar, as shown in Figs. 5 and 6. Some stratification was also visible in Al wire experiments[13] and has been reported as early as the 1960s in Cu and other wires (of much larger initial diameter than the wires we are studying here).[25,26] The cause of this stratification is believed to be a thermal instability. If small axial perturbations in the temperature exist, there will be perturbations in the wire resistivity. Regions with greater initial resistance are heated faster, and since the resistance increases with temperature, a thermal instability occurs, with the result that regions of initially higher resistance vaporize much faster. The initial perturbations might be grain boundaries, for example. However, we do not understand why this would result in such precisely planar structure as is observed in our radiographs.

Figure 11(a) shows a 1 μm insulated 25 μm Ag wire explosion radiographed at 318 ns. This is the only pulse out of 14 such pulses with this kind of wire in which the wire explosion was grossly nonuniform axially. One possible hypothesis explaining the difference in the expansion of the anode and cathode halves of the wire is a mm scale-length nonuniformity in the thickness of the insulation. Figure 11(b)

shows an expanded view of this wire near the center. A clear correlation is visible between the periodicity of the stratified layers and perturbations in the insulation layer along the right-hand side. Based on this, we infer that the regions between the more dense (darker) strata are filled with lower-density vapor as a result of more rapid expansion. It is worth noting that the periodicity of the stratified layers is similar to that of the perturbations visible in Fig. 9.

To determine whether initial nonuniformity existed as a result of the manufacturing process, and also to verify the wire diameters, the 25 μm Ag and 1 μm polyester-insulated 25 μm Ag wires were analyzed using a scanning electron microscope (SEM). The SEM images revealed no visible perturbations in wire diameter on the same scale as the observed stratification. Small pieces of dust or other imperfections were sometimes visible on the surfaces of the wires, but the imperfections were neither cylindrically symmetric nor did they appear with a periodicity correlating to the observed stratification. In addition, the wire diameters were equal to the manufacturer's values to within a few percent. In short, the exterior cold wire did not show any indications of nonuniformity caused by manufacturing imperfections.

The very early stages of wire explosions, up until the time of voltage collapse, are of interest if accurate information about the expansion just prior to voltage collapse can be obtained. The optical system had a diffraction limit near 20 μm, which severely limited it during the earliest stages of the wire explosions. In addition, the utility of the radiographs obtained at early times was limited to determining the boundary of the wire core; the internal wire core structure could not be discerned because the material areal density was still too high. Furthermore, the current and voltage diagnostics were susceptible to electrical noise generated in the diode region of the XP pulser system when early-time radiographs were obtained, making measurements of the current and voltage near the time of the x-ray bursts suspect. Finally, since the voltage collapse is believed to be the result of plasma formation around the wire, the use of the x-ray backlighting diagnostic at times near the voltage collapse time has the potential to hasten the voltage collapse process because of UV emission by the backlighter. In order to avoid all such problems, most of the backlighter pulses were timed to come after voltage collapse to ensure that the dynamics of the wire explosions would be determined by the LC1 pulser current and not the X-pinch UV emission.

The laser and x-ray data plotted in Fig. 4 for the various types of Ag wires are in close agreement. This need not be the case in general, however, because of the different minimum sensitivities of the two techniques. The x-ray backlighting images shown in Figs. 5 and 6 all included "step wedges" that were used to make calibrated mass density measurements, as discussed in Ref. 27. Each step is a known thickness of Ag deposited on the 12.5 μm Ti filters in the film cassettes [see Fig. 1(c)]. These allow us to absolutely calibrate the gray scale on each film with a known areal density of Ag. The thinnest step on the Ag step wedge was 0.05 μm, corresponding to an areal mass density of 52 μg/cm^2. This step was always resolvable, indicating that our minimum sensitivity level was less than this. In Ref. 13, we had found the minimum sensitivity level for Al was less than 60 μg/cm^2 but more than 30 μg/cm^2. The minimum sensitivity level of the laser interferometry is estimated to be 4×10^{16} cm^{-2} for electron plasma and 1.2×10^{17} cm^{-2} for Ag atoms (21.5 μg/cm^2). Experimentally, the laser and x-ray sensitivity levels appear to be comparable for Ag.

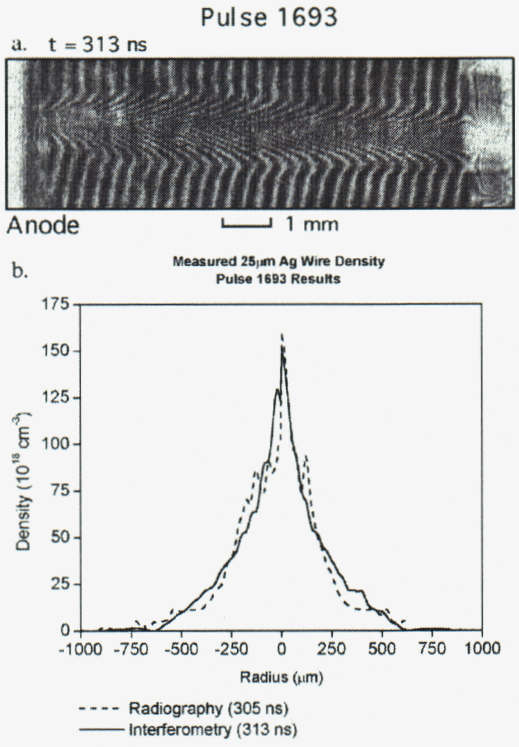

FIG. 12. (a) Interferometry image from pulse 1693, a bare 25 μm Ag wire explosion. (b) Atomic number densities estimated by analyzing the laser and x-ray images using Abel inversion are superimposed. Each half of the interferogram and radiograph images was analyzed independently, starting at $r=0$.

Using the calibrated step wedges for the x-ray backlighting images, it was possible to use Abel inversion techniques to find the mass density of the wire core as a function of the radius, from which the radial number density was inferred. Similarly, using the theoretical value for the polarizability of Ag,[28] the atomic number density of the wire core as a function of the radius was inferred from the laser interferometry images. These calculations were carried out for two typical 25 μm Ag wire explosions, pulses 1693 and 1694, and the results of these calculations are shown in Figs. 12 and 13, along with the interferometry images from these pulses for the bare Ag wires. The x-ray backlighting images (with step wedges) from those pulses are in Fig. 5. The inversion results are not symmetric about the axis because each half of the wire was Abel-inverted separately. The wire core density near the boundary obtained from the interferometry is likely too low, because the refractive index change due to a given plasma density can mask a neutral density of Ag about 3 times greater.

To compare the interferogram and radiograph results, the

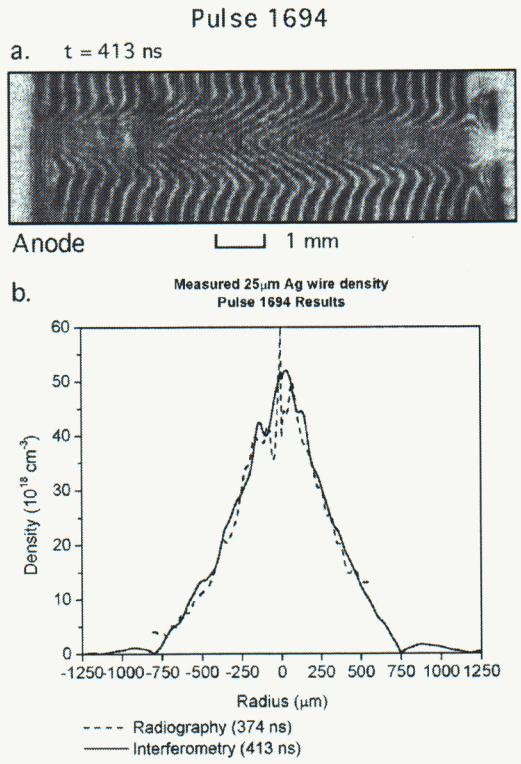

FIG. 13. (a) Interferometry image from pulse 1694, a bare 25 μm Ag wire explosion. (b) Atomic number densities estimated by analyzing the laser and x-ray images using Abel inversion are superimposed. Each half of the interferogram and radiograph images was analyzed independently, starting at $r=0$.

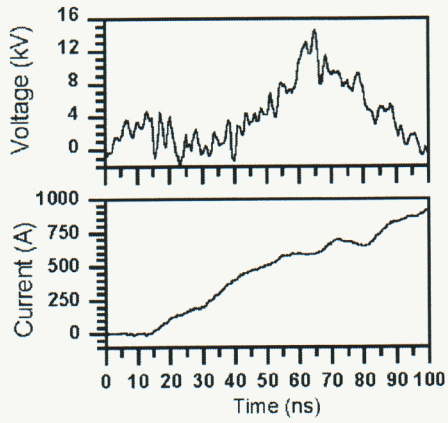

FIG. 14. Current and voltage applied to a 5 μm polyimide-insulated 25 μm W wire. The insulation near the electrodes was not mechanically stripped from the wire, as was normally the case for this wire. Note the voltage buildup of about 4 kV prior to current flow in the wire at about 14 ns. In addition, there are several abrupt voltage/current fluctuations at various times during the resistive phase, perhaps indicative of breakdowns along short segments of the wire.

waveforms in Figs. 12 and 13 were integrated to determine the number of atoms per unit length. All four of the Ag atom number density profiles in Figs. 12 and 13 (i.e., both the radiograph and interferometry waveforms in each figure), when integrated, corresponded to a linear number density of approximately 2.6×10^{17}/cm. The initial number of atoms per unit length of a 25 μm Ag wire is 2.85×10^{17}/cm. From these results we infer that the two diagnostics are measuring approximately 100% of the initial wire mass (to within our estimated measurement error of $\pm10\%$). The density profiles also agree relatively well, keeping in mind that the radiographs and interferograms are not simultaneous. In the future, we expect to be able to use a combination of these techniques to directly measure the polarizability of several metals.[29]

Two types of 25 μm diameter W wires were tested, bare wires and commercially available wires insulated with a 5 μm coating of polyimide. The first experiments with the insulated W wires revealed that the 5 μm thick polyimide layer prevented the electrical contact between the wire and the electrodes necessary for current to flow through the wire. Eventually, enough voltage would build up to puncture the insulating layer and current could flow through at least a portion of the wire. This can be seen in Fig. 14, which shows the current through and the voltage along an insulated 25 μm W wire (pulse 1657). Evidently, a voltage of around 4 kV was required to establish a current path through the insulation to the wire. Figure 15 contains an x-ray backlighting image from a similar pulse, in which it is clear that the wire did not expand uniformly along its axis. In every pulse in which no special precautions were taken to ensure initial electrical contact, very nonuniform expansion was observed, and the portion of the wire where expansion did occur was always at the cathode end of the wire. Thus, in all of the following insulated 25 μm W wire pulses presented in this paper, the insulation was carefully mechanically stripped from the contact region of the electrodes to improve the initial electrical contact.

It is readily apparent from Figs. 16 and 17 that the W wire explosions are markedly different from the Ag wire explosions. Figure 16 shows a series of radiographs of bare 25 μm W wire explosions at various times after the start of current flow in the wires. Figure 17 shows a similar series of x-ray backlighting images of the 25 μm W wires with the 5 μm coating of polyimide. As with Ag wires, the insulated W wire explosions appear to expand more rapidly than the bare W wires. Compared to the Ag wire explosions in Figs. 5 and 6, however, all of the W explosions are more axially nonuniform. This nonuniformity would make a graph of the maximum measured diameter vs. time for W potentially misleading.

The wire core expansion data obtained from the W radiographs is summarized in Fig. 18, with error bars determined as in Fig. 4. There are some important differences between Fig. 18 and Fig. 4, however. Because for Ag there is little axial variation in the diameter, the maximum measured wire core diameter is plotted as a representative number for the wire expansion in Fig. 4. This is not the case for the W wires. For 5 μm polyimide-insulated 25 μm W wires, we have plotted an axially averaged diameter obtained by measuring the dense wire core diameter at the same three axial positions in each image. The three axial points were sepa-

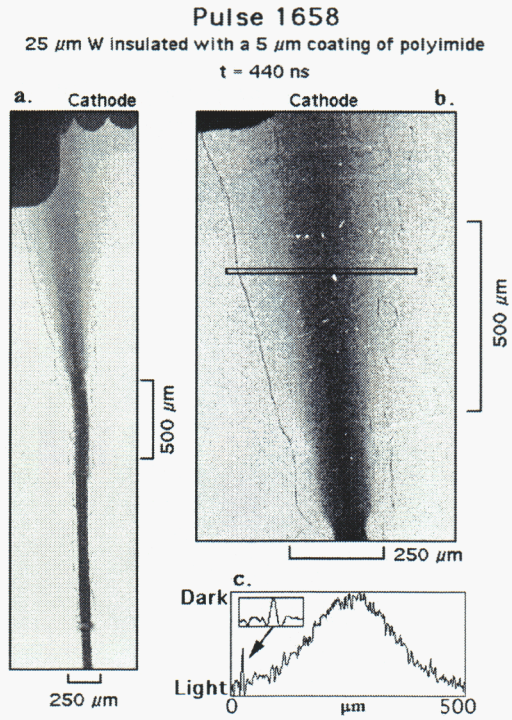

FIG. 15. (a) Radiograph image of the upper half of an exploding, 5 μm polyimide-insulated 25 μm W wire in which the polyimide insulation was not stripped from the W near the electrodes. (b) An expanded view of the upper part of (a). Note the fine structural detail of the insulation. (c) A film density profile of the boxed region showing refraction/reflection effects from the polyimide insulation, made clearer by expanding the region toward the left end of the profile in the box in the upper left-hand corner. These effects were visible at all axial positions along the insulation shown in b), not just the selected region.

rated by 2 mm and were chosen in the central region of the wire, away from the ends. (As the images in Figs. 16 and 17 show, the wires often expand significantly less near the electrodes, possibly due to current shunting by plasma formed near/at the contact points.) These three axial points were averaged to provide a single value for the measured diameter in that image. For bare 25 μm W explosions, the maximum

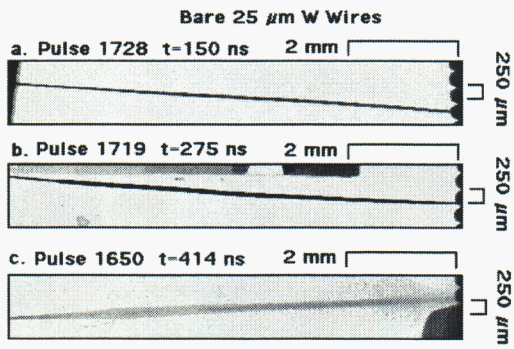

FIG. 16. X-ray radiographs of exploding, bare 25 μm W wires. Each image is from a different test pulse. The times given are relative to the start of the current flow in the wire: (a) 150 ns, (b) 275 ns, and (c) 414 ns.

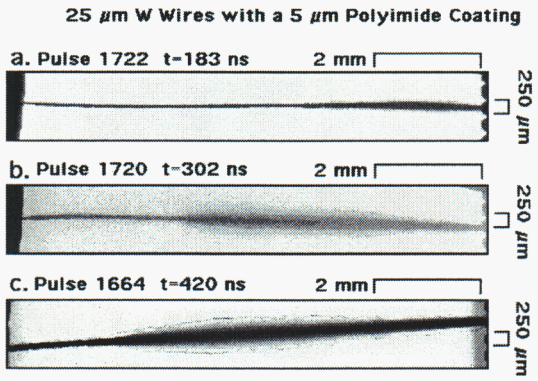

FIG. 17. X-ray radiographs of exploding, 5 μm polyimide-insulated 25 μm W wires. Each image is from a different test pulse. The times given are relative to the start of current flow in the wire: (a) 183 ns, (b) 302 ns, and (c) 420 ns.

measured diameter was plotted. This is because the bare 25 μm expansion was slow enough that the error in the estimated expansion rate includes both the axially averaged and maximum expansion cases.

Examining the results shown in Fig. 18, there is a clear difference in the behavior of the insulated and bare 25 μm W wires. At late times, the difference in expansion is quite marked. Interestingly, the time at which the expansion begins seems to show a wide variation for the insulated W pulses, and does not appear to start immediately following the voltage collapse. The reason for this is presumed to be that even with the insulation, the energy deposited in 25 μm W wires is still much less than the substantial vaporization energy for this material, as shown in Table III. Thus, only a fraction of the total mass can be vaporized and the remainder must remain in a liquid (or solid) state. The expansion rates obtained for the bare and insulated W expansion results shown in Fig. 18 were 0.29 ± 0.04 μm/ns and 1.6 ± 0.2 μm/ns, respectively.

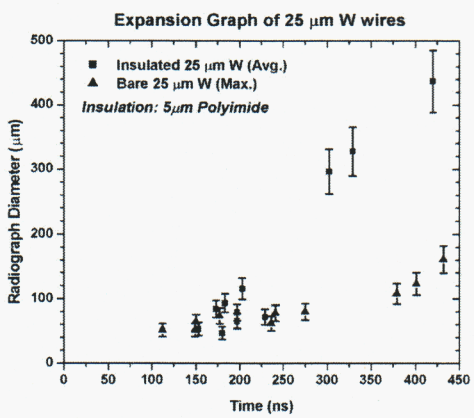

FIG. 18. Exploding W wire diameter vs time. For bare 25 μm W wires, the maximum measured wire diameter was plotted. For 5 μm polyimide-insulated 25 μm W wires, the diameters from three points in the central region of the wire were averaged together to yield an average wire diameter.

TABLE III. The measured energy deposition range indicates the minimum and maximum energy deposition values experimentally measured using current and voltage diagnostics. This energy is deposited in the wire during an initial resistive heating stage, as discussed in the text, and the duration of this phase is estimated to within ±2 ns from the current waveforms. The estimated total energy required to completely melt the wire starting from room temperature, including the latent heat of melting, is given in column 4. Column 5 gives the estimated total energy required to completely vaporize the wire starting from room temperature, including the latent heat of vaporization. The experimentally measured energy deposition values are expressed as a percentage of the vaporization energy in column 6. Core expansion rates measured using X-pinch radiography are given in the final column. An asterisk in column three indicates that <3 data points exist for that wire.

Wire diameter and material	Resistive phase duration (ns)	Measured energy deposition range (mJ)	Energy to melt the wire (mJ)	Energy to vaporize the wire (mJ)	Percent of vaporization energy deposited	Expansion rate of core diameter (cm/μs)
12.7 μm Al	34	23–38	3.7	41.6	55–91%	0.20±0.01
25 μm Ti	31	26*	27	277	9%	~0.03
25 μm Fe	39	60*	41	251	24%	-
25 μm Cu	71	88–112	28	237	37–47%	0.08 to 0.12
25 μm Cu (5 μm insul.)	93	330–470	28	237	139–198%	0.41 to 0.51
25 μm Zn	52	53–74	12.2	82.3	64–90%	0.24 to 0.6
25 μm Nb	40	55*	42.6	324	17%	-
25 μm Mo	43	47*	44	299	16%	~0.03
25 μm Ag	70	76–112	20	138	55–81%	0.45± 0.04
25 μm Ag (1 μm insul.)	85	310–420	20	138	225–304%	1.03± 0.05
25 μm Ag (5 μm insul.)	72	120–165	20	138	87–120%	0.51± 0.06
7.5 μm W	23	8–11*	5.6	39	21–28%	-
11.5 μm W	29	12–19*	13.2	91.7	13–21%	~0.013
11.5 μm W (2.2 μm insul.)	39	43–48*	13.2	91.7	47–52%	~0.2
12.5 μm W	32	22–45*	15.6	108	20–42%	-
25 μm W	43	35–62	42	432	8–14%	0.029± 0.004
25 μm W (5 μm insul.)	65–80	120–210	42	432	28–49%	0.16± 0.02
25 μm Pt	44	48–53	36.5	275	17–19%	-
12.7 μm Au	31	21*	5.6	44	48%	-
20 μm Au	50	55–80	14.4	113	49–71%	0.12 to 0.14
25 μm Au	64	79–94	22.5	176	45–53%	0.26 to 0.30

The voltage across, the current through, and the energy deposition in bare and 5 μm polyimide-insulated 25 μm W wires are plotted in Fig. 19. Once again, the primary effect of the insulating layer appears to be to prolong the resistive heating phase by postponing the voltage collapse that terminates it. Thus, more energy is deposited in the wire, resulting in faster expansion rates.

Figure 15 shows an example radiograph from a test in which the 5 μm polyimide was not removed from the contact points. Evidently, a breakdown occurred through the insulation at the point of contact between the wire and the electrode, but plasma formed around the insulated wire less than 1 mm from the electrode. Presumably together with a break in the insulation, this enabled the current to flow outside the wire relatively early in the pulse. Figure 14 shows the current and voltage waveforms for such a test. We observe that there appear to be numerous sudden fluctuations in the voltage and current waveforms that are not present in Ag waveforms (see Fig. 7). In addition, there is no sharp voltage collapse analogous to that seen in Ag wires, but rather a more gradual drop in the voltage. We speculate that this behavior is symptomatic of small breakdowns along short axial segments of the wire accompanied by breaks in the insulation. Such small breakdowns would shunt current away from the wire core in the region where they occurred, and may explain why the expansion of W wires is often very nonuniform. Of all the materials tested with the voltage and current monitors in place (see Table III), insulated W wires are the only ones for which the voltage does not collapse sharply, with the exception of the oil-coated W wire results shown in Ref. 14.

An obvious feature in images of the insulated W wire explosion images shown in Figs. 15 and 17 is the presence of the insulation. In Fig. 15(b) the image of the upper part of the wire has been expanded to show some of the details of the insulation. In Fig. 15(c), the film density profile of a section of this image has been plotted. This profile clearly shows the presence of thin layers of polyimide. On either side of these polyimide layers, narrow negative spikes are present. These spikes appear to represent regions where refraction due to the insulation, and/or reflection off the insulation surface, caused a sharp increase in x-ray photon intensity on either side of the insulation. From this we infer that the insulation visible at this time is still in solid form.

Similar refraction/reflection effects can be seen in Fig. 20(a), which shows a radiograph of a portion of a polyimide-insulated 25 μm W wire explosion 197 ns after the start of current flow in the wire. Figures 20(b)–20(d) show some film density profiles of this wire, indicating regions of high film exposure just to the outside of the opaque wire core. Figure 20 also suggests that if there is any vapor between the insulation and the expanding core, it is below our sensitivity limit.

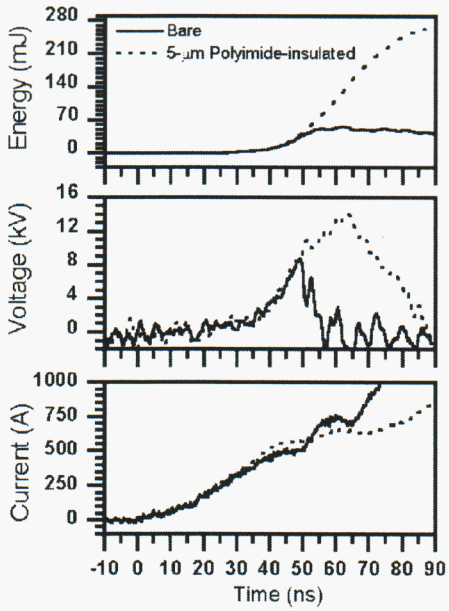

FIG. 19. The first 90 ns of the current and voltage applied to the W wires from the LC1 pulser, and the energy deposited in the wire. The two cases shown are bare and 5 μm polyimide-insulated 25 μm W wires.

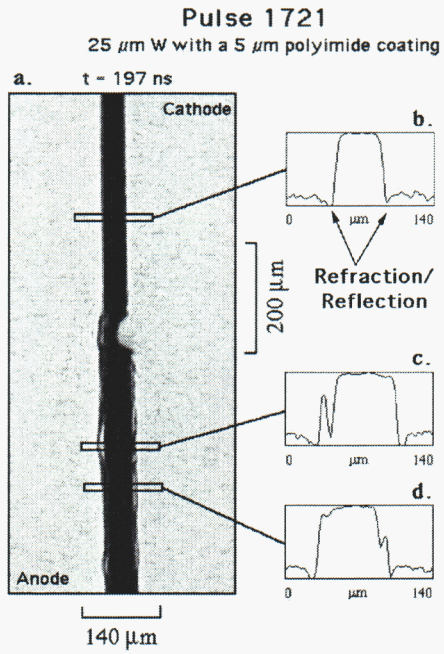

FIG. 20. (a) A radiograph of a 5 μm polyimide-insulated 25 μm W wire at $t=197$ ns. Intense bands of light on either side of the dense wire core are visible, indicative of refraction/reflection effects from the wire. (b)–(d) Film density profiles of selected wire segments showing a structure indicative of refraction/reflection. The gap between the wire core and the insulation is about 10 μm in the profile in (c).

Table III summarizes the energy deposition and expansion rate results from all wires tested with the voltage and current diagnostics. The energy required to completely vaporize the wire was estimated from data provided in Ref. 24. We note first that no bare materials had sufficient energy deposition during the resistive heating phase to exceed the amount of energy required to fully vaporize the wire. With insulating coatings, however, some wire materials did exceed the vaporization energy. Although we do not present radiographs of wire core expansion for all materials tested, we found that wire materials with a total energy deposition greater than 50% of the vaporization energy expand the fastest and have the most axially uniform expansion. By contrast, materials with small fractions of the vaporization energy deposited in them generally exhibit substantially axially nonuniform, relatively slow expansion.

A general trend of the wires listed in Table III is that high-conductivity, low boiling-point materials tend to expand the fastest and the most uniformly. Correspondingly, the energy deposition in these materials is usually a substantial fraction of the energy required to completely vaporize the wire. By contrast, highly resistive, high boiling-point materials such as W tend to exhibit more nonuniformity and expand more slowly. The energy deposition in these materials is also a small fraction of the energy necessary to completely vaporize them. The fact that Zn appears to expand well may suggest that the boiling point is the more important of these two parameters, as Zn has a very low boiling point but a room-temperature conductivity comparable to W.

Ag is an example of a material in the first class; it expands very fast and uniformly. The boiling point of Ag is relatively low, and it is a highly conductive metal, which may serve to keep the voltage drop along the wire low enough to delay breakdown relative to other materials. Silver also has the highest fraction of the vaporization energy deposited in it, as seen in Table III. An example of a material in the second class, in addition to W, is Ti, which according to Table III, typically receives only 9% of the energy required to completely vaporize it. Figure 21(a) shows a radiograph of the cathode end of two, 1-cm long, 25 μm Ti wires at $t=11$ μs. So little of the material was actually vaporized that the majority of the initial wire mass appears to be still be in its original location. This portion of the radiograph is representative of the entire length of the wire, which formed numerous 50–55 μm diameter droplets, from which we infer that the material heated up to the liquid state and stayed there. Images of two 25 μm Ti wires at 420 ns (not shown) indicate that the wires are the same diameter as those in Fig. 21(a), although the wire had not broken up into small droplets. Other similar images of materials at late times can be found in Ref. 12. This behavior contrasts sharply with Ag, which is almost completely invisible (i.e., below the minimum sensitivity level of the diagnostics) to the x-ray and optical diagnostics after about 1 μs due to its rapid expansion.

From the fact that substantial local nonuniformities are sometimes observed in materials that otherwise expand uniformly, we infer that there may be impurities or defects in the wires. Two examples of gaps in the dense wire core are shown in Fig. 21(b) for 1-cm long, 12.7 μm Al wires and 21(c) for a 1-cm long, 25 μm Zn wire. Clearly visible in the lower wire of Fig. 21(b) is a sharp gap in the dense wire core about 60 μ m across. The debris pattern visible on the anode/

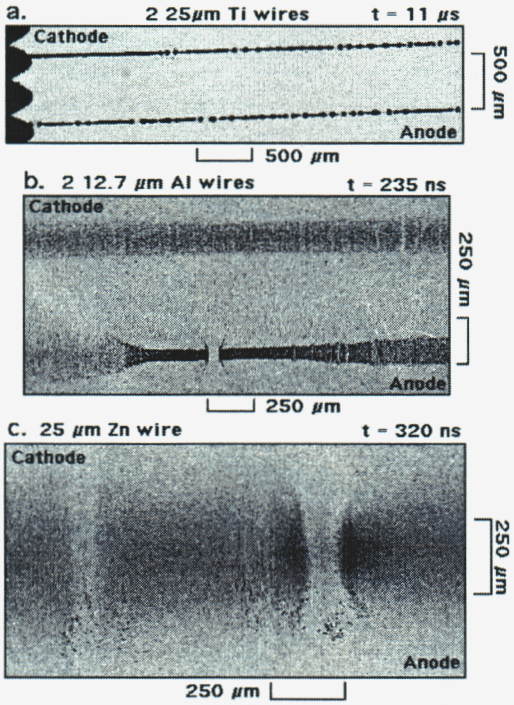

FIG. 21. (a) Radiograph of the cathode end of 2 exploded 25 μm Ti wires taken $t=11$ μs. Almost the entire length of the wire from the anode to the cathode shows the same pattern of droplets, all of which appear to be 50–55 μm in diameter. (b) Radiograph of the central region of 2 exploding 12.7 μm Al wires taken at $t=235$ ns, showing dense stratified layers in the wire and the presence of a large gap with sharply defined boundaries. Other than the gap region shown, both wires had expanded uniformly. (c) Radiograph of the central region of an exploding 25 μm Zn wire at $t=320$ ns. Two of the five gaps observed in this wire are shown. All of the gaps had small particles/droplets visible on the same side of the gaps (down in this image), with particle diameters ranging from 20 μm down to the resolution limit (<2 μm).

cathode edges of the gap indicates a radially outward explosion. Schlieren images (not shown) also indicate a gap in the wire. The lack of radial expansion along the wire near the gap is possibly due to current shunting by plasma formed in this region as a result of the explosion that created the gap. Similar current shunting is believed to occur in almost all wire materials near the electrode contact points. This mechanism would explain the lack of expansion near the anode and cathode visible in Figs. 5, 16, and 17 (see also Refs. 12 and 13 for examples of this phenomenon in other materials.) In the two gap regions of the Zn wire explosion shown in Fig. 21(c), small droplets are visible outside of the gap, toward the bottom of the figure, ranging in size from about 2 μm (resolution limit) to 20 μm. Three other gaps in this wire (not shown) also exhibited similar droplets that are visible on the same side of the gap. The random nature of these gaps makes it difficult to ascertain their cause experimentally.

As a final example of the complex structures often observed in our experiments we present in Fig. 22 a radiograph at $t=587$ ns of the cathode end of an exploding 11.5 μm W wire coated with about 2.2 μm of polyimide insulation. About 100 μm from the cathode end of the figure, below the

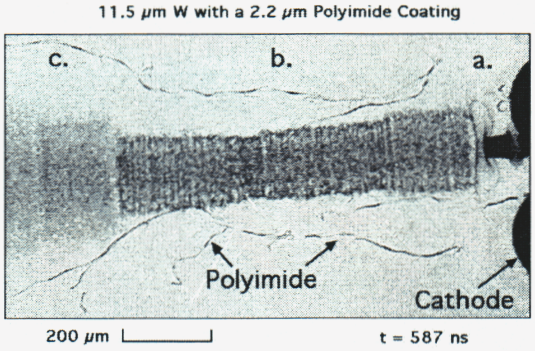

FIG. 22. Radiograph of the cathode end of an exploding 11.5 μm W wire coated with 2.2 μm of polyimide insulation, showing extreme axial variations in the wire expansion and behavior. Also visible is a gap near the cathode side of the radiograph similar to that seen in Fig. 21(b), as well as strands of the polyimide insulation blowing off the dense wire core.

"a," a gap in the wire exists that is reminiscent of the Al wire gap in Fig. 21(b). In this case, the radial expansion along the wire on either end of the gap is dramatically different, though both segments are expanded. The middle axial segment of the wire in Fig. 22, the segment below the "b," contains a foam-like structure with a sharp boundary, again similar to that seen in experiments using Al wires,[13] which we attributed to complex boiling processes. In the axial segment of the wire nearest the anode end of Fig. 22 ("c"), the W is significantly more expanded and has a very diffuse boundary. Also present in this segment and the central region of the same wire are faint stratified layers similar to those observed in Ag wires. The final feature of interest is the very nonuniform distribution of the strands of polyimide insulation, similar to that seen in Figs. 15, 17, and 20. Thus, we see that even W exhibits the same morphology as more rapidly expanding materials, but each "stage" occurs later in time and much more nonuniformly than with the rapidly expanding materials.

From radiographs such as Fig. 22 we infer that fairly extensive axial segments of exploding wires can have significantly different amounts of energy deposited in them. The consequence of this is that our estimates for the energy deposition per unit length are average values with a large standard deviation in many cases (especially for materials in which a small fraction of the vaporization energy is deposited, since they tend to have the most pathological behavior). Consequently, the behavior of wires such as W will be extremely difficult to model realistically starting from room temperature using computer codes.

IV. SUMMARY AND CONCLUSIONS

The principal result of this investigation is that the initial energy deposition as a fraction of the vaporization energy of the wire is highly correlated with the expansion rate, and if that fraction is close enough to 1, the wire core expansion is reasonably uniform. The insulating coatings provided a direct way of observing the importance of the resistive heating phase, since, by prolonging it, they can have a substantial effect on the expansion rate and uniformity of wire explo-

sions driven by prepulse-like conditions. The change in the energy per unit length as reflected in the expansion rates confirms the importance of the initial resistive heating phase. Once the current is shunted from the wire core due to presumed plasma formation along the wire, further direct heating of the core is negligible because the core resistance is so high relative to the surrounding plasma. Additional heating of the core is then limited to indirect deposition by radiation or thermal conduction from the surrounding plasma.

The use of thin, insulating coatings may hold promise for improving the energy deposition in many different wire materials and sizes under prepulse-like conditions. In Table III we presented results from experiments using insulated Ag, Cu, and W wires. Ongoing experiments with other wire materials, such as Pt and Au, indicate that insulating coatings have similar effects in these cases.[30] Thus, insulating coatings appear to be advantageous for many wire materials if rapid expansion is required. The use of insulating coatings in practice may be limited to relatively thin layers, however, as suggested by the W and Ag wire results presented in this paper. Establishing electrical contact between the wire and the electrodes was a problem in insulated 25 μm W wire explosions. This may also have contributed to the poor performance of 25 μm Ag wires insulated with 5 μm of polyester relative to 25 μm Ag wires insulated with 1 μm of polyester. This problem appeared to be remedied in the 25 μm W wire experiments by mechanically removing the insulation from the electrode regions, but this may not be practical for wire-array experiments. Chemical removal of the plastic at the contact point may be required if thicker insulating coatings are used.

The mechanism causing the voltage collapse along a wire is still not well understood. We postulate that plasma formation outside the wire core is responsible for the collapse, but have not directly observed the presence of this plasma. This is because the magnetic pressure in these experiments near the time of voltage collapse is insufficient to confine plasma surrounding the wire to a small enough channel and high enough density to be visible with our laser interferometer (minimum sensitivity $\sim 4\times 10^{16}$ cm^{-2}). For plasma to shunt enough current to cause a voltage collapse, it should have a resistance of less than 0.1 Ω. Assuming Spitzer resistivity, a uniform-density cylinder of plasma, and a plasma ionization state of ~ 1, we find a relationship for the plasma radius and temperature of $r^{-2}T^{-3/2}<0.1$, where r is the radius in mm and T is the electron temperature in eV. This relationship indicates that reasonable plasma parameters range from a 1 mm, ~ 10 eV plasma to a 0.1 mm, ~ 1 keV plasma. The first case would be near the lower detection limit of the optical interferograms if it were initiated from ~ 100 monolayers of hydrocarbons from the wire surface. The second case is well below our lower detection limit. Through the use of optical streak or frame photography, it may be possible to directly observe the formation and location of plasma outside the wire from its optical emission, and thus confirm when and in what region plasma formation occurs. Another possibility is the use of time-resolved optical spectroscopy to look for the presence of ions near the wire. We plan on making such measurements in the near future.

Our understanding of the situation with coatings is even more speculative at present. In several of the images we show here, especially with W (see Figs. 15 and 20), it appears that pressure may build up between the coating and the wire. Figure 11(b) for Ag also appears to support this conjecture. Therefore, it appears that the coating may keep the gases desorbed from the wire material from expanding to the point that an avalanche breakdown can occur. Simple estimates indicate that negligible resistive heating, heating by thermal conduction, or radiative heating occurs in the insulation, so we do not expect the coating to be a source of vapor unless, perhaps, an energetic electron-induced desorption leads to surface breakdown along the coating. In short, we do not understand how plasma can be formed within a large enough volume, and possibly pass through the insulator, to cause a voltage collapse. We note, however, that plasma forming along the wire is probably responsible for the voltage collapse along both bare and insulated wires, since in both cases the wire cores expand axially symmetrically, and the load resistance drops to "zero" at about the same rate.

In conclusion, we note that the current parameters used in the experiments here were chosen to simulate existing prepulse conditions on wire array experiments such as those performed on the Z-machine at Sandia National Laboratories, Albuquerque. They also apply to the beginning of the current pulse on the MAGPIE experiment at Imperial College. At present, the duration of the prepulse on the Z-machine is 50–100 ns. Given the resistive heating phase durations and the typical expansion rates for the materials studied to date (see Table III), it is likely that little wire expansion has taken place by the time the main current pulse on the Z-machine arrives. Work by Lebedev *et al.*[31] suggests that it should be possible to observe a difference in the behavior of wire-array implosions if the wires are allowed to expand to a diameter of about 1/3 of the interwire gap spacing. Using the data from Table III, we can estimate the minimum amount of time required for wires in a 300 wire, 2 cm diameter array to expand to a diameter of 1/3 of the interwire gap spacing (that is, to about 70 μm). As an example, we find that a bare 25 μm Ag wire would take at least 80 ns (70 ns for the resistive heating phase and 10 ns of expansion time) to expand to about 70 μm. By contrast, 1 μm polyester-insulated 25 μm Ag wires would take at least 90 ns to expand that far (85 ns plus 5 ns for expansion). Using examples more relevant to experiments to date on the Z-machine, it would take a bare 11.5 μm W wire over 480 ns to expand to 70 μm, but 11.5 μm W insulated with 2.2 μm of polyimide would take a minimum time of only 70 ns. We note, however, that that these estimates are made using the maximum expansion rates, so that materials such as W that expand very nonuniformly axially will require significantly more time before most of the wire length is sufficiently expanded. In all cases, we note that finer wires should take less time to meet this criterion, simply because the time required to heat the finer wires to the same temperature is reduced.

An obvious question is whether or not it is beneficial for the wires to expand significantly prior to the main pulse in a test on Z. At present, no experiments have been done to test

specifically whether a long prepulse or a delay between application of the prepulse and arrival of the main pulse (to permit significant wire expansion) would be advantageous. One possible disadvantage of significant expansion prior to the implosion is that the perturbations in each wire could become correlated more quickly during the implosion, as suggested by the experiments presented in Ref. 31.

The experiments presented in this paper, along with ongoing and future experiments, should ultimately prove useful for determining appropriate wire parameters for wire-array experiments, including whether wires should be coated with an insulator and/or be driven by a specially shaped prepulse. This could occur through trial-and-error with faster expanding wires in array experiments or by helping to validate computer codes that can then be used to predict the results of changing wire materials and/or using coatings.

ACKNOWLEDGMENTS

The authors wish to thank Dr. Jeremy Chittenden, Dr. Sergei Lebedev, Dr. Rick Spielman, and Dr. Mike Cuneo for their many helpful discussions on the experiments reported here. D.B.S. would like to thank Dr. Tom Sanford for a discussion during the 1999 International Conference on Plasma Science meeting that led to initial experiments with oil-coated wires.

This research was supported by Sandia National Laboratories, Albuquerque, Contract No. BD-9356 and Department of Energy Grant No. DE-FG03-98DP00217. Scanning electron microscopy of some of the wires presented here was done at the Cornell Center for Materials Research Shared Experimental Facilities, which is supported through the National Science Foundation Materials Research Science and Engineering Centers program (Award DMR-9632275).

[1]R. B. Spielman, S. F. Breeze, G. A. Chandler *et al.*, *Proceedings of the 11th International Conference on High-Power Particle Beams,* Prague, Czech Rep., 1996, edited by K. Jungwirth and J. Ullschmied (Czech Academy of Sciences, Prague, 1996), Vol. 1, pp. 150–153; R. B. Spielman, G. A. Chandler, C. Deeney *et al.*, Bull. Am. Phys. Soc. **41**, 1422 (1996).

[2]R. B. Spielman, C. Deeney, G. A. Chandler, M. R. Douglas, D. L. Fehl, M. K. Matzen, D. H. McDaniel, T. J. Nash, J. L. Porter, T. W. L. Sanford, J. F. Seaman, W. A. Stygar, K. W. Struve, S. P. Breeze, J. S. McGurn, J. A. Torres, D. M. Zagar, T. L. Gilliland, D. O. Jobe, J. L. McKenney, R. C. Mock, M. Vargas, T. Wagoner, and D. L. Peterson, Phys. Plasmas **5**, 2105 (1998).

[3]J. P. Apruzese, P. E. Pulsifer, J. Davis, R. W. Clark, K. G. Whitney, J. W. Thornhill, T. W. L. Sanford, G. A. Chandler, C. Deeney, D. L. Fehl, T. J. Nash, R. B. Spielman, W. A. Stygar, K. W. Struve, R. C. Mock, T. L. Gilliland, D. O. Jobe, J. S. McGurn, J. F. Seaman, J. A. Torres, and M. Vargas, Phys. Plasmas **5**, 4476 (1998).

[4]C. Deeney, C. A. Coverdale, M. R. Douglas, T. J. Nash, R. B. Spielman, K. W. Struve, K. G. Whitney, J. W. Thornhill, J. P. Apruzese, R. W. Clark, J. Davis, F. N. Beg, and J. Ruiz-Camacho, Phys. Plasmas **6**, 2081 (1999).

[5]T. W. L. Sanford, R. E. Olson, R. L. Bowers, G. A. Chandler, M. S. Derzon, D. E. Hebron, R. J. Leeper, R. C. Mock, T. J. Nash, D. L. Peterson, L. E. Ruggles, W. W. Simpson, K. W. Struve, and R. A. Vesey, Phys. Rev. Lett. **83**, 5511 (1999).

[6]R. J. Leeper, T. E. Alberts, J. R. Asay *et al.*, Nucl. Fusion **39**, 1283 (1999).

[7]T. J. Nash, M. S. Derzon, G. A. Chandler, R. Leeper, D. Fehl, J. Lash, C. Ruiz, G. Cooper, J. F. Seaman, J. S. McGurn, S. Lazier, J. Torres, D. O. Jobe, T. Gilliland, M. Hurst, R. Mock, P. Ryan, D. Nielson, J. Armijo, J. McKenney, R. Hawn, D. Hebron, J. J. McFarlane, D. Peterson, R. Bowers, W. Matsuka, and D. D. Ryutov, Phys. Plasmas **6**, 2023 (1999).

[8]S. N. Bland and S. V. Lebedev (private communication, 2000).

[9]R. E. Olson, J. L. Porter, G. A. Chandler, D. L. Fehl, D. O. Jobe, R. J. Leeper, M. K. Matzen, J. S. McGurn, D. D. Noack, L. E. Ruggles, P. Sawyer, J. A. Torres, M. Vargas, D. M. Zagar, H. N. Kornblum, T. J. Orzechowski, D. W. Phillion, L. J. Suter, A. R. Thiessen, and R. J. Wallace, Phys. Plasmas **4**, 1818 (1997).

[10]I. H. Mitchell, J. M. Bayley, J. P. Chittenden, J. F. Worley, A. E. Dangor, and M. G. Haines, Rev. Sci. Instrum. **67**, 1533 (1996).

[11]J. P. Chittenden (private communication, 2000).

[12]S. A. Pikuz, T. A. Shelkovenko, D. B. Sinars, J. B. Greenly, Y. S. Dimant, and D. A. Hammer, Phys. Rev. Lett. **83**, 4313 (1999).

[13]D. B. Sinars, T. A. Shelkovenko, S. A. Pikuz, J. B. Greenly, and D. A. Hammer, Phys. Plasmas **7**, 1555 (2000).

[14]D. B. Sinars, T. A. Shelkovenko, S. A. Pikuz, Min Hu, V. M. Romanova, K. M. Chandler, J. B. Greenly, D. A. Hammer, and B. R. Kusse, Phys. Plasmas **7**, 429 (2000).

[15]J. P. Chittenden, S. V. Lebedev, J. Ruiz-Camacho, F. N. Beg, S. N. Bland, C. A. Jennings, A. R. Bell, M. G. Haines, S. A. Pikuz, T. A. Shelkovenko, and D. A. Hammer, Phys. Rev. E **61**, 4370 (2000).

[16]P. Stoltz and T. Melhorn (private communication, 2000).

[17]D. B. Reisman (private communication, 1999).

[18]T. A. Shelkovenko, S. A. Pikuz, A. R. Mingaleev, and D. A. Hammer, Rev. Sci. Instrum. **70**, 667 (1999).

[19]T. A. Shelkovenko, D. B. Sinars, S. A. Pikuz, Ya. S. Dimant, K. M. Chandler, and D. A. Hammer, "Point-projection x-ray radiography using an X-pinch x-ray source," to be published in Rev. Sci. Instrum.

[20]D. H. Kalantar, Ph.D. dissertation (Cornell University, 1993).

[21]S. A. Pikuz, V. M. Romanova, N. V. Baryshnikov, Min Hu, B. R. Kusse, D. B. Sinars, T. A. Shelkovenko, and D. A. Hammer, "A simple air-wedge shearing interferometer for studying exploding wires," to be published in Rev. Sci. Instrum.

[22]R. B. Spielman and M. Cuneo (private communication, 2000).

[23]*Electrical Resistivity Handbook,* edited by G. T. Dyos and T. Farrel (Peter Peregrinus, London, U.K., 1992), p. 534.

[24]I. K. Kikoin, *Tables of Physical Values* (Atomizdat, Moscow, 1976).

[25]W. G. Chace, Phys. Fluids **2**, 230 (1959); W. G. Chace in *Exploding Wires,* edited by W. G. Chace and H. K. Moore (Plenum, New York, 1959), Vol. I, p. 7.

[26]K. S. Fansler and D. D. Shear, in *Exploding Wires*, edited by W. G. Chace and H. K. Moore (Plenum, New York, 1959), Vol. 4, p. 185.

[27]S. A. Pikuz, T. A. Shelkovenko, A. R. Mingaleev, D. A. Hammer, and H. P. Neves, Phys. Plasmas **6**, 4272 (1999).

[28]*CRC Handbook of Chemistry and Physics,* edited by David R. Lide, 78th ed. (CRC, New York, 1997), p. 10-201.

[29]M. Hu, D. B. Sinars, S. A. Pikuz, K. M. Chandler, J. B. Greenly, D. A. Hammer, B. R. Kusse, and T. A. Shelkovenko, *IEEE Conference Record 00CH37087* (Institute of Electrical and Electronics Engineers, Piscataway, NJ, 2000), p. 140.

[30]K. M. Chandler, M. Hu, D. B. Sinars, T. A. Shelkovenko, S. A. Pikuz, J. B. Greenly, D. A. Hammer, and B. R. Kusse, Ref. 29, p. 139.

[31]S. V. Lebedev, F. N. Beg, S. N. Bland, J. P. Chittenden, A. E. Dangor, M. G. Haines, S. A. Pikuz, and T. A. Shelkovenko, Phys. Rev. Lett. **85**, 98 (2000).